CHAPTER 15

Threshold Detection of Radar Targets

Mark A. Richards

Chapter Outline

15.1 INTRODUCTION

One of the most fundamental tasks of a radar is detection, the process of examining the radar data and determining if it represents interference only, or interference plus echoes from a target of interest. Once a target is detected, the system can turn its attention to processing the target information. Depending on the type of radar application, the system might be concerned with estimating the target radar cross section (RCS), measuring and tracking its position or velocity, imaging it, or providing fire control data to direct weapons to the target.

The basic concept of threshold detection was discussed in Chapter 3. Chapter 7 described common statistical models for the target echo power, including both probability distributions and pulse-to-pulse decorrelation models. Chapters 3 and 8 discussed coherent and noncoherent integration of data to improve the signal-to-noise ratio (SNR). In this chapter, these topics are brought together to provide a more detailed look at the optimal detection of fluctuating targets in noise. The analysis shows how the idea of threshold detection arises. The strategy for determining threshold levels and predicting detection and false alarm performance is demonstrated, and specific results are developed for the common Swerling target models. Also discussed are Albersheim's equation (first mentioned in Chapter 3) and Shnidman's equation, both very simple but useful analytical tools for estimating detection performance.

15.2 | DETECTION STRATEGIES FOR MULTIPLE MEASUREMENTS

15.2.1 Dwells and Coherent Processing Intervals

As discussed in Chapter 3, an individual target will generally be within the radar antenna mainbeam for a period of time, called the dwell time, that corresponds to a number of pulse repetition intervals (PRIs). That is, the radar may "hit" the target with multiple pulses during a dwell time. The data obtained during a dwell time might be organized into one or more coherent processing intervals (CPIs). Chapter 3 also showed that radar targets are generally detected using a threshold test procedure and that the best detection performance for a given P_{FA} is obtained if the signal-to-noise ratio of the data to be tested is maximized before the threshold test.

A CPI of coherent radar data and its organization into a fast-time/slow-time data matrix is shown in Figure 15-1. Each individual sample is a complex (in-phase [I] and quadrature [Q]) measurement of the amplitude and phase of the received echo signal. The gray shaded set of samples are the slow-time samples for a single range bin. Assuming no *range migration* (see Chapter 21), all of the echoes from a particular target in a CPI of data will be in a single range bin. If there are multiple CPIs in the dwell time, there will be multiple data matrices.

The term *coherent processing interval* suggests that the data within the CPI will be combined coherently, that is, using both amplitude and phase information. While this will usually be true, it is also possible to combine CPI samples noncoherently. Thus, the term CPI implies a block of coherent radar data but does not necessarily imply a specific means of combining that data.

At the point of threshold detection, a single value derived from the available data is compared with a threshold value and a decision made. The quantity to which the threshold test is applied is called the *detection statistic*.

15.2.2 Coherent, Noncoherent, and Binary Integration

The signal-to-noise ratio (SNR) of the detection statistic is often improved relative to that of a single target-plus-noise sample by *integrating* (adding) the multiple measured samples of the target and noise, motivated by the idea that the interference can be "averaged out" and the target echo reinforced by adding multiple samples. Thus, in general detection will be based on N samples of the combined target-plus-interference signal.

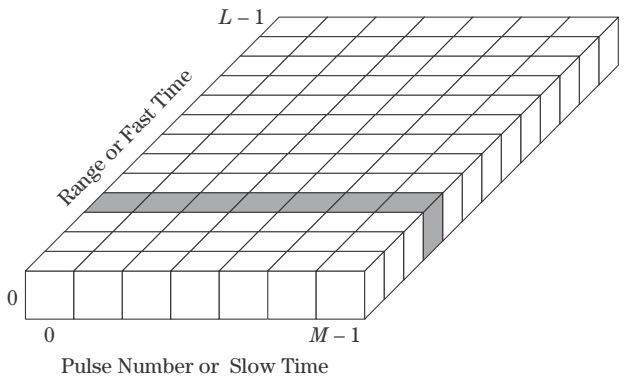

FIGURE 15-1 ■ One CPI of fast-time/slow-time data. The shaded region is the echo samples for the fourth range bin.

At least three types of integration may be applied to the data:

1. After coherent demodulation, to the baseband complex-valued (I and Q, or magnitude and phase) data. Combining complex data samples is referred to as *coherent integration*.
2. After envelope detection of the complex data, to the magnitude (or squared or log magnitude) data. Combining magnitude samples after the phase information is discarded is referred to as *noncoherent integration*.
3. After threshold testing, to the target present/target absent decisions. This technique is called *binary integration*, *m-of-n detection*, or *coincidence detection*.

In coherent integration, complex (magnitude and phase) data samples y_n are combined to form a new complex variable y:

$$y = \sum_{n=1}^{N} y_n e^{j\phi_n} \tag{15.1}$$

The phase weights $\exp(j\phi_n)$ are chosen to compensate the phase of the data samples y_n so that they add in phase with one another. If the SNR of a single complex sample y_n is χ_1 and the interference is uncorrelated from sample to sample, the coherently integrated complex data sample y has an SNR that is N times that of the single sample, that is, $\chi_N = N\chi_1$ (where χ_N and χ_1 are in linear units). That is, coherent integration attains an *integration gain* of N.

Coherent integration is effective only if the N data samples have a predictable phase relationship so that appropriate phase compensation can be applied in equation (15.1). Modern radar systems offer several opportunities for coherent integration. The most important ones were indicated in Figure 14-8, which showed the subsets of a coherent datacube used for various coherent operations. Depending on the particular system, the coherent operations used may include pulse compression of fast-time samples, pulse-Doppler processing of slow-time samples, and beamforming across phase centers. Synthetic aperture radar (SAR) imaging and space-time adaptive processing coherently integrate two-dimensional (2-D) subsets of the datacube.

For example, in pulse-Doppler processing, phase compensation of the data within a CPI for stationary and moving targets is typically accomplished with a K-point discrete Fourier transform (DFT) of the slow-time data, forming a range-Doppler map and effectively testing K different phase compensation functions corresponding to different Doppler shifts at once as discussed in Chapter 14. Applying the DFT is effective only if the pulses are collected at a constant pulse repetition interval (PRI) over a relatively short time interval. Doppler processing details are given in Chapter 17, and SAR is discussed in Chapter 21.

Noncoherent integration takes place after envelope detection, when phase information has been discarded. Instead, the magnitude or squared magnitude of the data samples is integrated. (Sometimes another function of the magnitude, such as the log magnitude, is used.) For example, noncoherent integration with a square law detector bases detection on the detection statistic

$$z = \sum_{n=1}^{N} |y_n|^2 \tag{15.2}$$

Both linear and square law detectors are considered in this chapter; the choice is primarily for convenience in discussing various topics. Noncoherent integration of N samples provides an integration gain less than N but greater than about $\sqrt{N}$.

Binary integration takes place after an initial detection decision has occurred on each of several CPIs of data. Because there are only two possible outputs of the detector each time a threshold test is made, the output is said to be binary. Multiple binary decisions can be combined in an "m-of-n" decision logic in an attempt to further improve performance. That is, a detection is not declared unless the target is detected in m of the n threshold tests. This type of integration was discussed in Chapter 3.

15.2.3 Data Combination Strategies

A system could elect to use none, one, or any combination of these integration techniques. Many systems use at least one integration technique, and a combination of either coherent or noncoherent with postdetection binary integration is common. The major costs of integration are the time and energy required to obtain the multiple datacube samples to be integrated and the computation required to combine those samples. The collection time is time that cannot be spent searching for targets elsewhere, or tracking already-known targets, or imaging other regions of interest. Modern systems vary as to whether the computational load is an issue: the required operations are simple but must be performed at a very high rate in many systems. Chapter 3 included examples of the trade-offs between different integration options within a given timeline in determining detection performance.

Suppose a radar collects two CPIs of data within a single dwell with two pulses per CPI and 5 range bins per pulse, giving a total of 20 data samples.[1] One processing approach would coherently integrate all 20 samples, giving a single integrated sample with a 13 dB integration gain compared with any one sample alone. There would be a single detection statistic (the magnitude or magnitude squared of the integrated sum) and a single threshold test. This strategy for detection testing of the available data is diagrammed in Figure 15-2a. In this figure, small white boxes indicate coherent (amplitude and phase) data samples, while gray boxes indicate noncoherent (magnitude or magnitude squared only, no phase) samples. The hexagons with an inscribed $\times$ are the detection statistic, the quantity to be tested against the threshold.

The phase relationship between the data in two different CPIs is generally not known, so the approach of Figure 15-2a is generally not practical. A very practical approach is to coherently integrate the data in fast time (pulse compression) and slow time (Doppler DFTs) within each CPI separately. Within a single CPI, the peak of the Doppler DFT in the range bin of interest would represent the coherently integrated target echo for the 10 samples of that CPI and would exhibit an integration gain of 10 dB. The values of the two resulting Doppler spectrum peaks could then be noncoherently integrated, producing a gain of at least 1.5 but less than 3 dB in the noncoherently integrated sample compared with the individual Doppler spectrum peaks. This again gives a single detection statistic that includes both coherently and noncoherently combined data and has an SNR gain greater than 10 dB but less than 13 dB, as compared to the SNR of a single sample. Figure 15-2b illustrates this approach.

[1] More realistic numbers would be perhaps three to eight CPIs per dwell, a few tens of pulses per CPI, and hundreds of range bins per pulse. The smaller numbers in this example are used to simplify Figure 15-2.

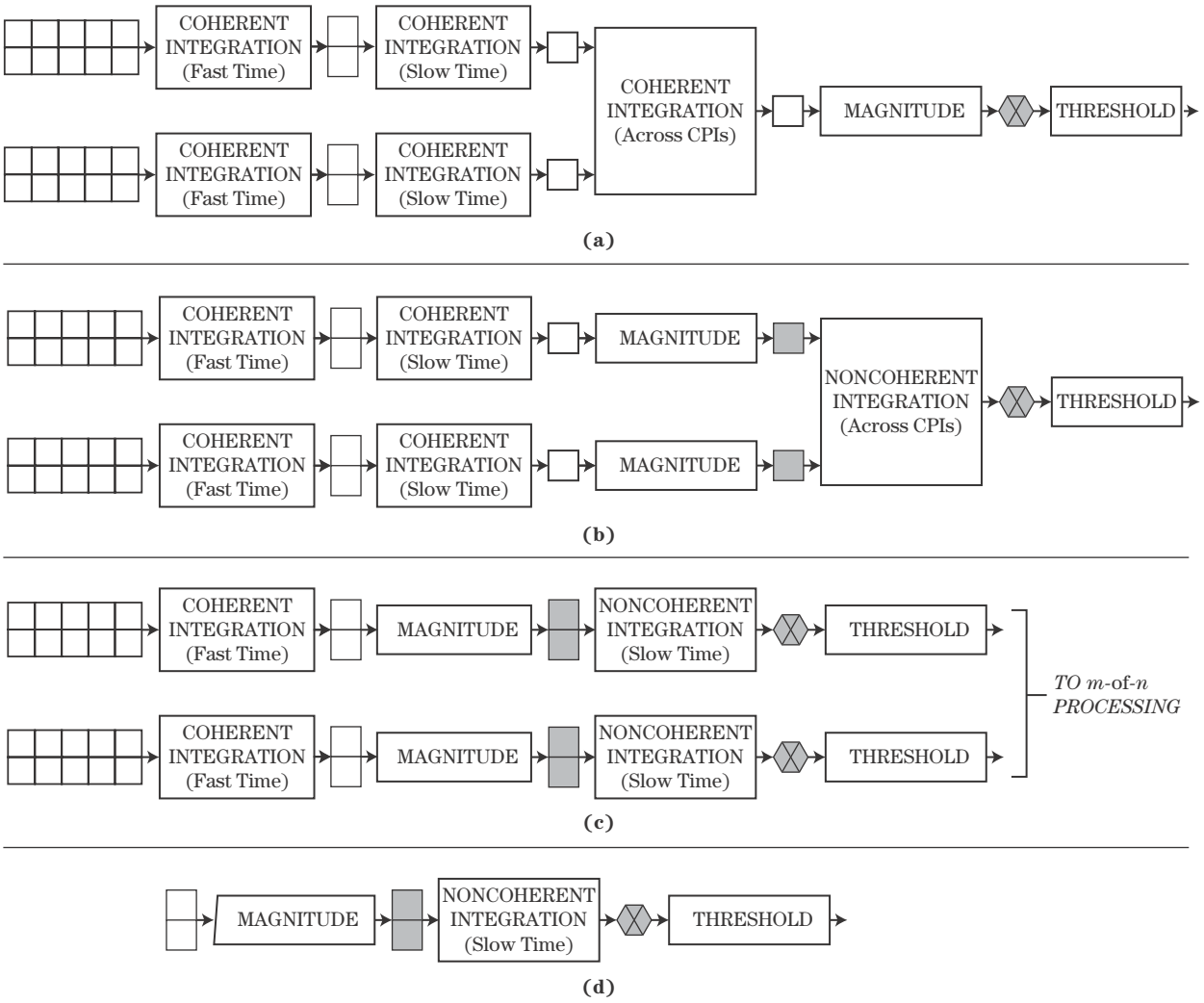

FIGURE 15-2 ■ Alternative detection strategies. (a) Coherent integration of all data. (b) Noncoherent integration of coherently integrated CPIs. (c) Mixed integration and threshold testing within each CPI followed by m-of-n detection. (d) Noncoherent integration only in slow time for a single range bin.

Figure 15-2c illustrates one version of the binary integration approach. Coherent integration in fast time and noncoherent integration in slow time are performed within a CPI to form a detection statistic, and then a threshold detection test is applied to each CPI separately. In this example, this would produce two separate target/no-target decisions. These could then be combined in a logic that declares a detection only if the target in that range bin was detected on at least one of the individual CPIs. (A more realistic example might require detection on perhaps two of five or three of eight CPIs.) Another version of this approach (not shown) would replace noncoherent integration in slow time with coherent integration (Doppler DFTs) prior to the threshold test and binary integration.

Figure 15-2d illustrates a simpler system that does not use pulse compression to effect coherent integration in fast time. In this case, samples from a given target are confined to

a single range bin. Integration is in slow time only and can be coherent or noncoherent; the noncoherent case is diagrammed here.

Other combinations of coherent and noncoherent are also possible. Of the scenarios illustrated in Figure 15-2, cases (b) and (d) are the most common. Case (a) is unrealistic because of the lack of a known phase relationship between CPIs. Case (c) is not unreasonable, but it is more likely that coherent integration would be used in slow time if possible.

The purpose of the analysis in this chapter is to provide the tools to determine the probability of detection P_D for a given probability of false alarm P_{FA} for many of these scenarios so that the best processing strategy for the available data can be determined. It will be seen that the detection performance will depend on the number of data samples integrated before the threshold test, the combination of coherent and noncoherent integration strategies applied to those samples, the SNR of the samples, and the target fluctuation model that describes the target echo component of the samples.

15.3 INTRODUCTION TO OPTIMAL DETECTION

A single echo sample of radar data is composed of either interference alone or interference plus target echoes. The interference is, at a minimum, receiver noise, and might also include air or ground clutter echoes, electromagnetic interference (EMI) from other transmitting sources (e.g., radars, television stations, cellular telephones), and hostile jamming. The signals received from these interference sources are modeled as additive random processes, as discussed for clutter in Chapter 5. Thus, even if the target echo amplitude is entirely deterministic, the combined target-plus-interference signal is a random process.

15.3.1 Hypothesis Testing and the Neyman-Pearson Criterion

For any radar measurement that is to be tested for the presence of a target, one of two hypotheses can be assumed true:

1. The measurement is the result of interference only.
2. The measurement is the combined result of interference and echoes from a target.

The first hypothesis is denoted as the *null hypothesis,* H_0, and the second as H_1. A statistical description of the data under each hypothesis is needed. For simplicity, assume initially that this is a single echo sample (one fast-time sample from a single pulse) denoted y. Then two probability density functions (PDFs) $p_y(y|H_0)$ and $p_y(y|H_1)$ are required:

$p_y(y|H_0)$ = PDF of y given that a target was *not* present

$p_y(y|H_1)$ = PDF of y given that a target *was* present

Design of the detection algorithm and analysis of the resulting radar performance is dependent on developing models for these PDFs for the system and scenario at hand. Furthermore, a good deal of the radar system design problem is aimed at manipulating these two PDFs to obtain the most favorable detection performance.

The detection logic must examine each radar measurement to be tested and select one of the hypotheses as "best" accounting for that measurement. If H_0 best accounts for the data, then the system declares that a target was not present at the range, angle, or Doppler coordinates of that measurement; if H_1 best accounts for the data, then the system declares

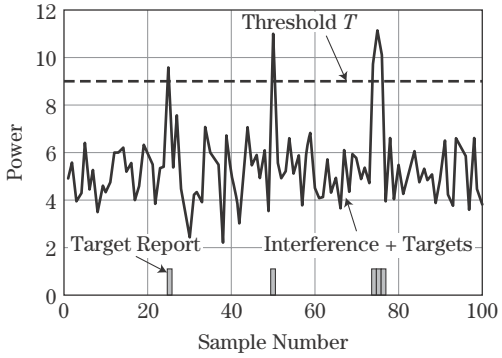

FIGURE 15-3 ■ The concept of threshold detection.

that a target was present.[2] The best procedure to use depends on the definition of "optimal" and the details of the random process models that describe the data.

Radar detection algorithms are usually designed according to the *Neyman-Pearson criterion*, a particular optimization strategy. This rule fixes the probability of false alarm, P_{FA}, that will be allowed by the detection processor and then maximizes the probability of detection, P_D, for a given SNR. Applying the Neyman-Pearson criterion to realistic radar detection problems leads to threshold detection using various detection statistics determined by the particular statistics of the data [1]. The threshold detection procedure is illustrated in Figure 15-3. The radar data shown could be received power versus range for a single pulse, or the Doppler power spectrum at a given range, or even a row of pixels in a SAR image. Whatever its source, a threshold value T is computed, and each data sample is compared with that threshold. If the sample is below the threshold, it is *assumed* to represent interference only. If it is above the threshold, it is similarly assumed to be too strong to represent interference only. In this case it must be interference plus a target echo, so a detection is declared at the range, velocity, or image location represented by that sample.

It is important to realize that these decisions can be wrong! A strong interference spike can cross the threshold, leading to a *false alarm*. Given a good model of the interference, the threshold can be selected to control the false alarm probability, P_{FA}. Similarly, a weak target echo might not add enough power to the interference to cause it to cross the threshold so that the target is not detected; this is called a *miss*, and its probability is $1 - P_D$.

The achievable combinations of P_D and P_{FA} are affected by the quality of the radar system and signal processor design. However, it will be seen that for a fixed system design, increasing P_D implies increasing P_{FA} as well. The radar system designer will generally decide what rate of false alarms can be tolerated based on the implications of acting on a false alarm, which may include overloading an operator monitoring a radar detection screen, using radar resources to start a track on a nonexistent target, or in extreme cases even firing a weapon!

Denote the number of detection decisions per unit time (usually 1 second) made by a particular radar as N_D. The *false alarm rate* (FAR), *FAR*, is the average number of false alarms per unit time. N_D, P_{FA}, and *FAR* are related according to

$$FAR = N_D P_{FA} \tag{15.3}$$

[2] In some detection problems, a third hypothesis is allowed: "don't know." Most radar systems, however, force a choice between "target present" and "target absent" on each detection test.

Since a radar may make tens or hundreds of thousands, even millions of detection decisions per second, values of P_{FA} must generally be quite low to maintain a tolerable FAR. Values in the range of 10^{-4} to 10^{-8} are common, and yet may still lead to false alarms every few seconds or minutes. Higher-level logic implemented in downstream data processing, for example in the tracking algorithms described in Chapter 19, is often used to reduce the number or impact of false alarms.

15.3.2 The Likelihood Ratio Test

It is shown in most detection texts that, given a particular data measurement y, the Neyman-Pearson criterion leads to the decision rule [2]

$$\frac{p_y(y|H_1)}{p_y(y|H_0)} \underset{H_0}{\overset{H_1}{\gtrless}} T_\Lambda \tag{15.4}$$

where T_Λ is an as yet unknown threshold value. Equation (15.4) is known as the *likelihood ratio test* (LRT). It states that the ratio of the two PDFs, each evaluated for the observed data y to produce a single numerical value (this ratio is called the *likelihood ratio* [LR]), should be compared with a threshold. If the likelihood ratio exceeds the threshold, choose H_1, that is, declare a target to be present. If it does not exceed the threshold, choose H_0 and declare that a target is not present. It will soon become clear that the LRT implicitly specifies the data processing operations to be carried out on the observed data y; what exactly those required operations are will depend on the particular PDFs. Example operations include taking the magnitude of the data or coherently or noncoherently integrating multiple samples.

The following notation is common shorthand for the LRT:

$$\Lambda(y) \underset{H_0}{\overset{H_1}{\gtrless}} T_\Lambda \tag{15.5}$$

where $\Lambda(y) = p_y(y|H_1) \,/\, p_y(y|H_0)$. Going a step further, because the decision depends only on whether the LRT exceeds the threshold, any monotone increasing operation can be performed on both sides of equation (15.5) without affecting which values of observed data y cause the threshold to be exceeded and therefore without affecting the performance (P_D and P_{FA}). Most common is to take the natural logarithm of both sides of equation (15.5) to obtain the *log-likelihood ratio test*:

$$\ln \Lambda(y) \underset{H_0}{\overset{H_1}{\gtrless}} \ln T_\Lambda \tag{15.6}$$

Some specific examples will be developed shortly to make clearer the use of the LRT and log-LRT.

The likelihood ratio Λ is the ratio of two random variables and so is also a random variable with its own probability density function, $p_\Lambda(\Lambda)$. If a specific model for $p_\Lambda(\Lambda)$ can be found (this is usually difficult), then P_{FA} can be expressed in terms of that PDF as

$$P_{FA} = \int_{T_\Lambda}^{+\infty} p_\Lambda(\Lambda) d\Lambda \tag{15.7}$$

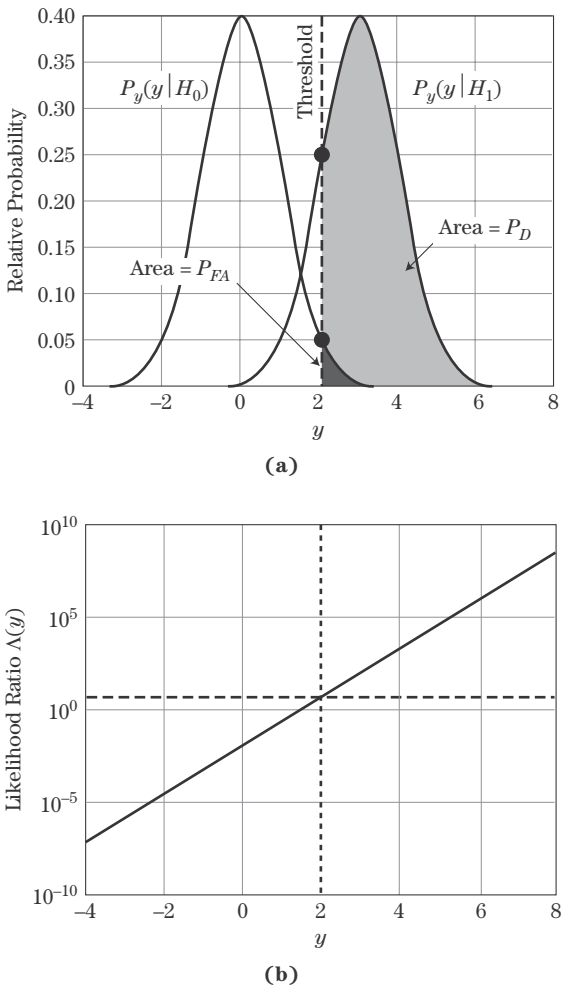

FIGURE 15-4 ■ (a) Notional Gaussian probability density functions of the voltage y under H_0 (left) and H_1 (right). The black area represents P_{FA} and the gray + black area P_D. (b) Likelihood ratio for the PDFs of part (a). See text for discussion.

This equation can then be solved for T_Λ. More commonly, P_{FA} is found by determining a model for the PDF of the detection statistic z under H_0 (interference only) and then finding a threshold value T such that probability of y exceeding T is the desired P_{FA}:

$$P_{FA} = \int_{T}^{+\infty} p_z(z|H_0)dz \tag{15.8}$$

Figure 15-4 illustrates the relationship among the PDFs of the data, the likelihood ratio, and the thresholds T and T_Λ for a simple case. Suppose the noise is a single sample of a real-valued zero-mean Gaussian random process with variance σ_n^2, while the signal is simply a constant value of m.[3] Thus the target-plus-noise random process is Gaussian with a mean of m and a variance σ_n^2. The detection statistic is just the single data sample y. The PDFs $p_y(y|H_0)$ and $p_y(y|H_1)$ for the case $m = 3$ and $\sigma_n^2 = 1$ are shown in Figure 15-4a.

[3]These are not realistic models of the PDFs of radar data but are for illustration only. More realistic PDFs are considered in Section 15.4.

The signal-to-noise ratio is $\chi = m^2/\sigma_n^2 = 9$ (9.5 dB). A threshold T is shown as a vertical line at $y = 2$. P_D and P_{FA} are the areas under the right and left PDFs, respectively, from T to $+\infty$. T is found by adjusting the position of the threshold until the black area equals the acceptable false alarm probability. The detection probability is then the gray area (which includes the black area). In this example, $P_{FA} = 0.0228$ and $P_D = 0.841$.

The likelihood ratio $p_y(y|H_1)/p_y(y|H_0)$ for this example is shown in Figure 15-4b. The value of the noise-only PDF at the data threshold value, $p_y(2|H_0)$, is 0.054, while that of the target-plus-noise PDF, $p_y(2|H_1)$, is 0.252. These two values are indicated by the small circles on the dotted line in Figure 15-4a. The likelihood ratio at this point is therefore $\Lambda(2) = 0.252/0.04 = 4.48$, as shown by the intersection of the two dotted lines in Figure 15-4b. Thus, applying a threshold of $T = 2$ to the measured data y is equivalent to applying a threshold $T_\Lambda = 4.48$ to the likelihood ratio in this example.

Figure 15-4a makes it clear that P_D and P_{FA} both increase as the data threshold T moves left and decrease as it moves right. The achievable combinations of P_D and P_{FA} are determined by the degree to which the two distributions overlap. To achieve a high P_D and a low P_{FA} at the same time, the two PDFs must be well separated so that they overlap very little and the threshold value can be placed between them.

Figure 15-5 illustrates one form of the *receiver operating characteristic* (ROC) curve for this problem. A ROC curve is a plot of two of the three quantities P_D, P_{FA}, and SNR with the third as a parameter. Figure 15-5 plots P_D versus P_{FA} with the SNR χ as a parameter. For a given P_{FA}, P_D increases as SNR increases, a result which should also be intuitively satisfying.

If the achievable combinations of P_D and P_{FA} do not meet the performance specifications, what can be done? Consideration of Figure 15-4 suggests two answers. First, for a given P_{FA}, P_D can be increased by causing the two PDFs to move farther apart when a target is present. That is, the presence of a target must cause a larger shift in the mean, m, of the distribution of the detection statistic. Since the SNR is m^2/σ_n^2, this is equivalent to stating that one way to improve the detection/false alarm trade-off is to increase the SNR. The second way to improve the performance trade-off is to reduce the overlap of the PDFs by reducing their variance, that is, by reducing the noise power, σ_n^2. As with the first technique of increasing m, this is equivalent to increasing the signal-to-noise ratio. Thus, improving the trade-off between P_D and P_{FA} requires increasing the SNR χ. This is a fundamental result that will arise repeatedly.

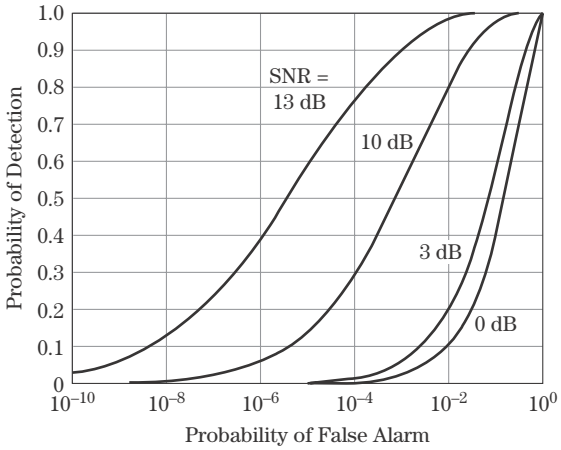

FIGURE 15-5 ■ Receiver operating characteristic for the Gaussian example for various values of the SNR.

Radar systems are designed to achieve specified values of P_D and P_{FA} subject to various conditions, such as specified ranges, target types, and interference environments. The designer can work with antenna design, transmitter power, waveform design, and signal processing techniques, all within cost and form factor constraints. The job of the designer is therefore to develop a radar system design that ultimately results in a pair of "target absent" and "target present" PDFs at the point of detection with a small enough overlap to allow the desired P_D and P_{FA} to be achieved. If the design does not do this, the designer must redesign one or more of the previously mentioned elements to reduce the variance of the PDFs, shift them farther apart, or both until the desired performance is obtained. Thus, a significant goal of radar system design is controlling the overlap of the noise-only and target-plus-noise PDFs, or equivalently, maximizing the SNR.

15.4 | STATISTICAL MODELS FOR NOISE AND TARGET RCS IN RADAR

The case of a real constant "target" in real Gaussian noise is not a realistic model for radar signals. In this section, more appropriate PDFs for describing radar interference and target statistics are reviewed. The concepts discussed in the preceding section can then be applied using these PDFs to estimate radar detection performance.

15.4.1 Statistical Model of Noise

The thermal noise at the output of each of the I and Q channels of a coherent radar receiver is typically modeled as a zero-mean Gaussian random process with variance $\sigma_n^2/2$. The I channel noise and the Q channel noise are assumed independent of each other. Under these circumstances, the complex noise signal $w[n] = I + j\mathrm{Q}$ is a complex Gaussian noise process, often called a *circular* random process, with zero mean and a variance that is just the sum of the I and Q channel variances, namely, σ_n^2.

Define z as the magnitude of this noise (the signal at the output of a linear detector). It is a standard exercise in many random process textbooks to show that the PDF of z has a Rayleigh distribution [3],

$$p_z(z) = \begin{cases} \dfrac{2z}{\sigma_n^2} \exp\left(\dfrac{-z^2}{\sigma_n^2}\right), & z \geq 0 \\ 0, & z < 0 \end{cases} \quad \text{(linear detector)} \tag{15.9}$$

If z is instead the squared magnitude of the complex Gaussian noise (i.e., the signal at the output of a square law detector), the detected noise has an exponential PDF,

$$p_z(z) = \begin{cases} \dfrac{1}{\sigma_n^2} \exp\left(-\dfrac{z}{\sigma_n^2}\right), & z \geq 0 \\ 0, & z < 0 \end{cases} \quad \text{(square-law detector)} \tag{15.10}$$

For either detector type, the PDF of the noise phase θ is uniform,

$$p_\theta(\theta) = \begin{cases} \dfrac{1}{2\pi}, & -\pi \leq \theta < \pi \\ 0, & \text{otherwise} \end{cases} \tag{15.11}$$

15.4.2 Statistical Models of Radar Cross Section for Targets

A variety of probability density functions have been proposed for modeling target RCS fluctuations; the most common of these were discussed in Chapter 7. For each model, there is a corresponding PDF for the target reflectivity, which is proportional to the square root of the RCS. Received echo power is proportional to the target RCS, while echo voltage is proportional to the reflectivity. Tables 7-1 and 7-2 list some of the common PDFs used to model target RCS and reflectivity, respectively. These included the nonfluctuating, exponential, and fourth-degree chi-square. The choice of PDF to model the RCS fluctuations directly affects predicted detection performance, as will be seen in Section 15.5.

15.4.3 RCS Decorrelation Properties

Detection decisions are often based not on a single measurement but on a set of N measurements. For instance, the received complex voltage from a particular range bin might be measured on a series of N pulses. As suggested by the results in Section 15.3, combining all N measurements to improve the SNR before performing the threshold test will improve performance relative to using only one measurement.

When N target measurements are combined, the question arises as to whether their amplitudes or powers should be modeled as a single value selected from the target PDF repeated N times, N different values selected from the target PDF, or something in between. The first case is referred to as *scan-to-scan decorrelation* (because the target echoes do not decorrelate within a single "scan" or CPI), while the second is referred to as *pulse-to-pulse* decorrelation. In many situations, the actual decorrelation behavior may lie between these two extremes, but they make useful bounding cases for performance prediction.

The concept of pulse decorrelation can also be applied across CPIs as well as within them. Suppose the data within a CPI are coherently integrated and the magnitude of the result computed. This process can be repeated for each of N CPIs and the N results noncoherently integrated to form the final detection statistic. In this scenario, detection performance would depend on whether the target RCS decorrelated from CPI to CPI rather than from pulse to pulse.

RCS decorrelation is due to changes in radar-target aspect angle or radar frequency during the time interval over which the N data samples are collected. The choice of decorrelation model will be important in predicting detection performance in Section 15.5. As was shown in Chapter 7, the change in aspect angle required to decorrelate the echo amplitude of a complex target can be estimated as

$$\Delta\theta = \frac{c}{2L_w f} \quad \text{radians} \tag{15.12}$$

where L_w is the size of the target normal to the radar-target line of sight (LOS), that is, the width of the target as viewed from the radar.

It was also shown that successive target samples will be uncorrelated with one another if the radar frequency is changed. The frequency step required to decorrelate a complex target is approximately

$$\Delta f = \frac{c}{2L_d} \quad \text{Hz} \tag{15.13}$$

where L_d is the depth of the target projected along the radar boresight. Some systems deliberately change the radar frequency from pulse to pulse, a process called *frequency*

agility, to ensure decorrelation of the target returns [4]. The reason for this will become apparent in Section 15.5.10. Frequency agility is not used within a CPI for the purpose of affecting the RCS decorrelation model if coherent integration is going to be applied to the CPI data.

As an example, consider a target the size of an automobile, about 2 m wide by 5 m long. At L-band (1 GHz), the target signature can be expected to decorrelate with between 30 and 75 mrad of aspect angle rotation (about 1.7° to 4.3°), depending on the target orientation. At W-band (95 GHz), this is reduced to only 0.316 to 0.79 mrad (0.018° to 0.0452°). The maximum frequency step required for decorrelation, which occurs when the target is viewed along its shortest axis, is 75 MHz. This value does not depend on the transmitted frequency.

The idea of target decorrelation (more generally, target fluctuations) is typically applied only in the context of noncoherent integration. Coherent integration usually occurs over relatively short time intervals, and the target is generally considered to exhibit constant RCS over the coherent integration time. Noncoherent integration often, though not always, occurs over longer time periods (e.g., multiple CPIs) that are more likely to result in observable RCS fluctuations. In some processing that requires long integration times, such as synthetic aperture imaging (see Chapter 21), target decorrelation can become a limiting factor.

15.4.4 Swerling Models

To model the performance of a radar detector, a model of the statistical behavior of the target RCS is required, including both a PDF and a decorrelation model. In combination with the noise model, the RCS model in turn determines the statistical model for the received voltage or power. As discussed in Chapter 7, *Swerling models* are one common set of target RCS models [5]. The Swerling models combine either the exponential or fourth-degree chi-square PDF with either the scan-to-scan or pulse-to-pulse decorrelation model. The exponential RCS model describes the behavior of a complex target consisting of many scatterers, none of which is dominant. The fourth-degree chi-square RCS model is an approximation to the *second-degree non-central chi square* (NCCS2) PDF that models targets having many scatterers of similar strength with one dominant scatterer. Table 15-1 defines the four cases. The terminology is sometimes stretched to include the nonfluctuating target case as the "Swerling 0" or "Swerling 5" model.

Choosing a Swerling model for analysis requires that a choice be made between the two PDFs and between the two decorrelation models. To choose the PDF, a judgment is needed as to whether the target RCS at the aspect angles of interest are likely to be dominated by one or two large scatterers or whether it is better described as the result of an ensemble of roughly equal scatterers. The choice of decorrelation model results from analyzing the geometry and motion of the radar and target over the CPI to determine whether the aspect

TABLE 15-1 ■ Swerling Models

Probability Density Function of RCS	Decorrelation	
	Scan-to-Scan	Pulse-to-Pulse
Exponential	Case 1	Case 2
Chi-square, degree 4	Case 3	Case 4

angle will change by an amount greater than $\Delta\theta$ during the CPI. If not, scan-to-scan decorrelation would be expected. If the aspect angle change between one target sample and the next is greater than $\Delta\theta$, then pulse-to-pulse decorrelation would be an appropriate model. If the time required to change the aspect angle by $\Delta\theta$ is greater than the time between successive samples, but less than the total CPI duration, the target decorrelation behavior will fall between the scan-to-scan and pulse-to-pulse limiting cases. In that case, calculations can be done for both cases and used to bound the range of detection results.

15.4.5 Extended Models of Target RCS Statistics

The concept of the Swerling models can easily be extended to other target models. For example, a model could be defined that uses a log-normal PDF for the target fluctuations with either pulse-to-pulse or scan-to-scan decorrelation to relate the N pulses in a block. Empirical observations have shown that such "long-tailed" distributions are often a better representation of observed radar data statistics than the traditional exponential and chi-square models, especially in high-resolution systems. Small-resolution cells are more likely to isolate one or a few scatterers, undermining the many-scatterer assumption of the traditional models and making large variations in observed RCS more likely. Detection probabilities for such models are sometimes difficult to develop, though a number of results are available in the literature (e.g., [6]). Other common models include the "expanded Swerling models" described in Chapter 7, which use the noncentral gamma density to make it possible to more closely match the density function to experimentally observed statistics for a wide range of systems while maintaining the (relatively) tractable computational results obtainable with target models based on chi-square and gamma densities [7,8].

15.4.6 Statistics of Targets in Interference and the Detection Statistic

The discussion of the aforementioned target models does not quite provide the information needed to carry out detection calculations. The data that will be subjected to the threshold detector will be the sum of the target echo and the interference, which is at least receiver noise and may also include clutter, jamming, and EMI. Thus, the probability density function of the target-plus-interference signal must be known. Furthermore, as shall be seen shortly, the optimum detector for N data samples will call for coherent or noncoherent integration of those samples followed by comparison of the resulting detection statistic to a threshold. Thus, the PDF of the sum of N outputs of the envelope detector when both target and interference are present will be needed.

15.5 THRESHOLD DETECTION OF RADAR SIGNALS

The models of the target and interference signals can now be used to develop equations for the performance of a radar detection scheme. Several basic choices distinguish common radar detection schemes:

- First, will detection be based on a single fast-time sample or multiple samples? In the latter case, are the data organized into one or several CPIs? Using multiple samples requires more radar resources to collect and process the data but obtains better results for a given single-sample SNR.

- What integration strategies will be used? There are three choices: coherent, noncoherent, and binary integration. Combinations of any two, or even all three, are also possible; four of these combinations were illustrated in Figure 15-2.
- If using noncoherent integration, what type of single-sample envelope detection law will be used? Common choices are linear and square law, as will be seen shortly; log detectors are also used.
- What target fluctuation model will be assumed? This requires specification of both a probability density function and a decorrelation model for the target samples. (Note that if detection is based on a single sample, decorrelation models are irrelevant.)
- Finally, will detection be based on a fixed threshold or on an adaptive threshold that responds to changes in the interference level? Adaptive threshold techniques are discussed in Chapter 16; here only fixed threshold detection will be considered.

In this section, the optimum detector under the Neyman-Pearson criterion for a nonfluctuating target, a single pulse, and a fixed threshold will first be presented. Next, the result for N samples of data with a predictable phase relationship will be developed, showing how coherent integration arises in detection. These results are then expanded to $N > 1$ samples with an unknown phase relationship for a nonfluctuating target, introducing noncoherent integration into the detection processing. Finally, the results are extended to include all four Swerling models of target RCS fluctuation.

15.5.1 Unknown Parameters

Realistic radar signals have unknown parameters. In most systems, the interference power is not known a priori. In this chapter it will be assumed that it is known, but Chapter 16 will show how to estimate it from the data and how that process affects detection performance. The range, amplitude, and Doppler shift of a target echo cannot be known before it has been detected. Even once detected, its exact phase will be unknown. Recall from Chapter 8 that the phase shift, θ, of the echo from a target at range R_0 is $-4\pi R_0/\lambda$ radians. Knowing the exact phase of the target echo implies knowing the range to the target very precisely, since a variation in one-way range of only $\lambda/4$ causes the received echo phase to change by 180°. At microwave frequencies, this is typically only 15 to 30 cm (at L-band to ultra high frequency [UHF]) to a fraction of a centimeter (at millimeter wave frequencies). To complicate matters further, some parameters are linked. For example, the unknown echo amplitude varies with the unknown echo arrival time according to the appropriate version of the radar range equation. Thus, the LRT must be generalized to develop a technique that can work when some signal parameters are unknown.

15.5.2 The Optimum Detector for Nonfluctuating Radar Signals, One Sample

The PDFs used in Figure 15-4 were not realistic models of even the simplest radar detection scenario. Assume a coherent system, so that both I and Q channels are present and that the noise in each channel is independent and identically distributed (IID) zero-mean Gaussian noise with variance $\sigma_n^2/2$. The total noise power is then just the sum of the I and Q noise powers, which is σ_n^2.

Assuming a nonfluctuating target simply means that, when present, it adds a complex constant $m = \tilde{m}\exp(j\theta)$ to the noise sample y. "Nonfluctuating" means that the target

RCS is a constant so that the amplitude of the target component of the echo signal, $\tilde{m}$, is also constant. Because the target echo phase is extremely sensitive to small variations in range, the phase angle, θ, of the target component of the measured data is modeled as a random variable distributed uniformly over $(0,2\pi)$ and independent of the amplitude $\tilde{m}$.

To carry out the LRT, it is necessary to return to its basic definition of equation (15.4) and to determine $p_y(y|H_0)$ and $p_y(y|H_1)$ A detailed derivation of these PDFs is beyond the scope of this chapter; see [2] for details. The result for a single complex noise sample is

$$p_y(y|H_0) = \frac{1}{\pi\sigma_n^2}\exp\left[-|y|^2/\sigma_n^2\right] \tag{15.14}$$

As expected, the PDF depends only on $|y|$. Since the target echo is not present under H_0, neither the target amplitude nor phase appears in equation (15.14).

For the nonfluctuating target-plus-noise case, $p_y(y|H_1)$ must be determined, considering the effect of the random target phase, θ. The *Bayesian approach* for random parameters with known PDFs is applied to "average out" the θ dependence, resulting in a PDF that depend only on the magnitude of the data. The result is the Rician PDF [2]

$$p_y(y|H_1) = \frac{1}{\pi\sigma_n^2}\exp\left[-\frac{1}{\sigma_n^2}\left(|y|^2+\tilde{m}^2\right)\right] I_0\left(\frac{2\tilde{m}|y|}{\sigma_n^2}\right) \tag{15.15}$$

where $I_0(\cdot)$ is the modified Bessel function of the first kind. Note that $p_y(y|H_1)$ uses only the magnitude $\tilde{m}$ of the complex signal sample but not the random phase of the target echo due to the averaging over θ.

The log-likelihood ratio is convenient in this case. It is straightforward to show that the log-LRT becomes

$$\ln\Lambda = \ln\left[\frac{p\,(y|H_1)}{p\,(y|H_0)}\right] = \ln\left[I_0\left(\frac{2\tilde{m}|y|}{\sigma_n^2}\right)\right] - \frac{\tilde{m}^2}{\sigma_n^2} \underset{H_0}{\overset{H_1}{\gtrless}} \ln T_\Lambda \tag{15.16}$$

Moving the term $\tilde{m}^2/\sigma_n^2$ to the right-hand side isolates the detection statistic on the left-hand side of the equation and gives a threshold test using a modified threshold T',

$$\ln\left[I_0\left(\frac{2\tilde{m}|y|}{\sigma_n^2}\right)\right] \underset{H_0}{\overset{H_1}{\gtrless}} \ln T_\Lambda + \frac{\tilde{m}^2}{\sigma_n^2} \equiv T' \tag{15.17}$$

Equation (15.17) defines the signal processing required for optimum detection in the presence of an unknown phase using a single complex data sample. It calls for taking the magnitude of the data sample, scaling it and passing it through the memoryless nonlinearity $\ln[I_0(\cdot)]$ to get the detection statistic, and comparing the result with a threshold.

As discussed previously, the phase is not the only unknown parameter of the target echo signal in practice. In this example, the amplitude $\tilde{m}$ of the echo depends on all of the factors in the radar range equation, including especially the unknown target radar cross section and, at least until it is successfully detected, the target's range. In addition, the target may be moving relative to the radar so that the echo is modified by a Doppler shift. It is straightforward to show that accounting for unknown target echo amplitude neither requires any change in the detector structure nor changes its performance [2]. The same is true of a Doppler shift in the single-sample case.

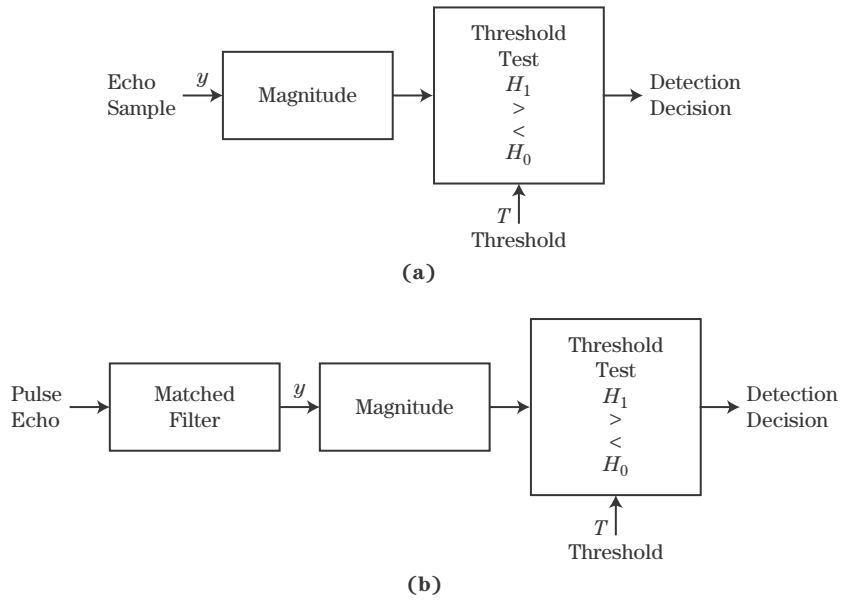

FIGURE 15-6 ■ Structure of optimal detector when the absolute signal phase is unknown.

15.5.3 Performance for the Nonfluctuating Signal in Gaussian Noise, $N = 1$

As a practical matter, it is desirable to avoid having to compute the natural logarithm and Bessel function in equation (15.17) for every threshold test, since these might occur millions of times per second in some systems. Because the function $\ln[I_0(\cdot)]$ is monotonic increasing, the same detection results can be obtained by simply comparing its argument $x = 2\tilde{m}|y|/\sigma_n^2$ with a modified threshold. After some further rearrangement, equation (15.17) then becomes simply

$$|y| \underset{H_0}{\overset{H_1}{\gtrless}} T \tag{15.18}$$

A detector that bases its decision on $|y|$ is called a *linear detector*, as opposed to a *square law detector* that would use $|y|^2$. Figure 15-6 illustrates the resulting optimal detector for the coherent receiver with an unknown phase. The matched filter maximizes the SNR of the complex data sample y; the linear detector and threshold test implement the LRT.

The performance of this detector will now be established. Let $z = |y|$. The detection test becomes simply $z \gtrless T$; thus, the distribution of z under each of the two hypotheses is needed. Under H_0 (target absent), the real and imaginary parts of y are IID Gaussian random processes with zero mean and variance $\sigma_n^2/2$, denoted as $\mathrm{N}\left(0, \sigma_n^2/2\right)$.[4] It follows from Section 2.2.6 of [2] that z is Rayleigh distributed:

$$p_z(z|H_0) = \begin{cases} \dfrac{2z}{\sigma_n^2} \exp\left(-\dfrac{z^2}{\sigma_n^2}\right), & z \geq 0 \\ 0, & z < 0 \end{cases} \tag{15.19}$$

[4]The notation N(u, v) denotes a normal (Gaussian) distribution of mean u and variance v.

The probability of false alarm is therefore

$$P_{FA} = \int_{T}^{+\infty} p_z(z|H_0)dz = \exp\left(-\frac{T^2}{\sigma_n^2}\right) \tag{15.20}$$

This equation can be inverted to obtain the threshold setting in terms of P_{FA}:

$$T = \sigma_n \sqrt{-\ln P_{FA}} \tag{15.21}$$

Equation (15.21) gives a rule for setting the threshold at the output of a linear detector to achieve the specified P_{FA}, assuming the noise power at the detector input is known.

Now consider H_1, (i.e., target present). The real part of y is distributed as $\mathrm{N}(\tilde{m}\cos\theta, \sigma_n^2/2)$, while the imaginary part is distributed as $\mathrm{N}(\tilde{m}\sin\theta, \sigma_n^2/2)$. It is shown in Section 2.2.7 of [2] that the PDF of z is

$$p_z(z|H_1) = \begin{cases} \dfrac{2z}{\sigma_n^2}\exp\left[-\dfrac{1}{\sigma_n^2}\left(z^2+\tilde{m}^2\right)\right] I_0\left(\dfrac{2\tilde{m}^2 z}{\sigma_n^2}\right), & z \geq 0 \\ 0, & z < 0 \end{cases} \tag{15.22}$$

Equation (15.22) is the Rician PDF. The probability of detection is obtained by integrating it from T to $+\infty$. It is convenient to make the substitutions $t = z\Big/\sqrt{\sigma_n^2/2}$ and $\alpha = \sqrt{2\tilde{m}^2/\sigma_n^2}$ to put the integral in the more standard form

$$Q_M(\alpha, t) = \int_{T}^{+\infty} t\exp\left[-\frac{1}{2}(t^2+\alpha^2)\right] I_0(\alpha t)dt \tag{15.23}$$

The expression $Q_M(\alpha, t)$ is known as *Marcum's Q function*. It arises frequently in radar detection calculations. A closed form for this integral is not known. An example of a MATLAB program for evaluating it iteratively is given in [2]. A comparison of several numerical algorithms for its computation is given in [9].

In terms of Marcum's Q function, the probability of detection is

$$P_D = Q_M\left(\sqrt{\frac{2\tilde{m}^2}{\sigma_n^2}},\ \sqrt{\frac{2T^2}{\sigma_n^2}}\right) \tag{15.24}$$

Finally, noting that $\tilde{m}^2/\sigma_n^2$ is the signal-to-noise ratio χ and expressing the threshold in terms of the false alarm probability using (15.21) gives

$$P_D = Q_M\left(\sqrt{2\chi},\ \sqrt{-2\ln P_{FA}}\right) \tag{15.25}$$

The performance of this detector for a nonfluctuating target in Gaussian noise is given in Figure 15-7. The general behavior is very similar to the real-valued constant-in-Gaussian-noise case of Figure 15-5.

A more interesting comparison is to the optimum coherent detector that would have been obtained if the target echo phase was known exactly. Although the equations are not derived here (see [1]), the resulting ROC is shown in Figure 15-8a. Again, the general shape of the performance curves is very similar to that of the envelope detector in Figure 15-7. Close inspection, however, shows that for a given SNR χ and P_{FA}, the coherent detector

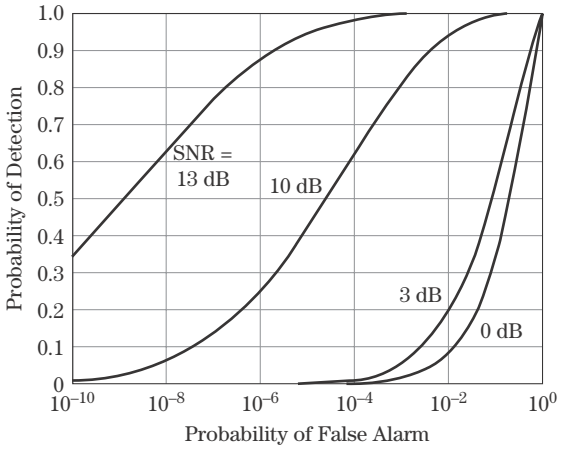

FIGURE 15-7 ■ Performance of the linear envelope detector for the Gaussian example with unknown phase.

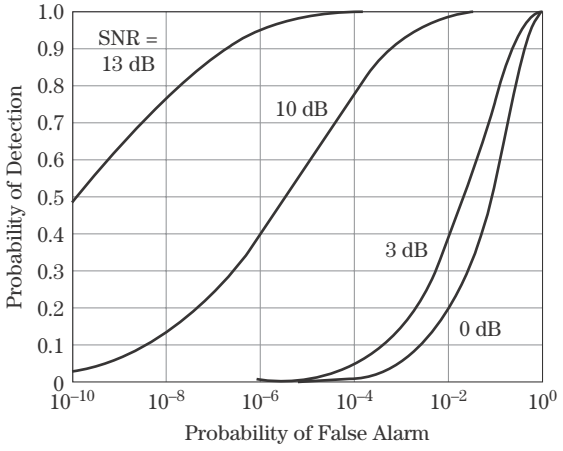

(a)

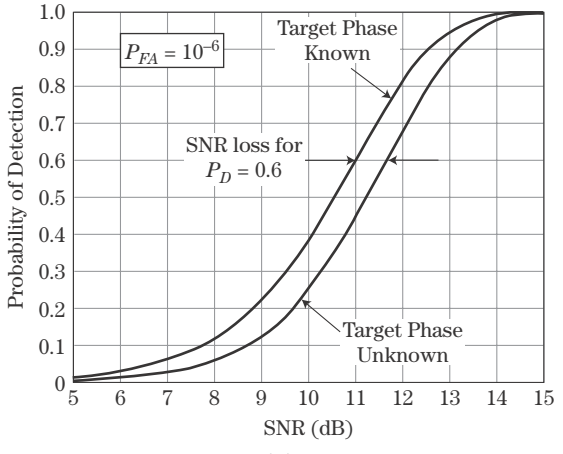

(b)

FIGURE 15-8 ■ (a) ROC for a coherent detector with known target phase (compare to Figure 15-7). (b) Detector loss due to unknown target phase.

obtains a higher P_D. This occurs because the coherent detector uses more information about the signal, namely, its phase.

To make this point clearer, Figure 15-8b plots the detection performance as a function of χ with P_{FA} fixed (at 10^{-6} in this example) for both the known and unknown phase cases (coherent and linear detectors). This figure shows that, to achieve the same probability of detection, the linear envelope detector requires about 0.6 dB higher SNR than the coherent detector at $P_D = 0.9$ and about 0.7 dB more at $P_D = 0.5$. The extra signal-to-noise required to maintain the detection performance of the envelope detector compared with the coherent case is called an *SNR loss*. SNR losses can result from many factors; this particular one is often called the *detector loss*. It represents extra SNR that must be obtained in some way if the performance of the envelope detector is to match that of the ideal coherent detector. Increasing the SNR in turn implies one or more of many radar system changes, such as greater transmitter power, a larger antenna gain, and reduced range coverage.

The phenomenon of detector loss illustrates a very important point in detection theory: the less is known about the signal to be detected, the higher must be the SNR to detect with a given combination of P_D and P_{FA}. In this case, not knowing the absolute phase of the signal has cost about 0.6 dB. Inconvenient though it may be, this result is intuitively satisfying: the worse the knowledge of the signal details, the worse the performance of the detector should be.

15.5.4 Optimum Detector for Nonfluctuating Radar Signals with Coherent Integration

In many cases the raw data contain more than one sample of data from the same target, and those data have a distinct phase relationship. For example, suppose the available data are N slow-time samples from a range bin containing a target moving at constant radial velocity with respect to the radar. As discussed in Chapter 8, a model for the slow-time target-only data $s[m]$ for the range bin of interest is

$$s[m] = Ae^{j(2\pi f_d mT+\theta)} = Ae^{j\theta}e^{j2\pi f_d mT}, \quad 0 \le m \le N-1 \tag{15.26}$$

where θ is the phase due to the target range on the first sample. These N samples of data can be compactly expressed as an $N \times 1$ column vector $\boldsymbol{S}$ of the form

$$\begin{aligned} \boldsymbol{S} &= Ae^{j\theta}\left[\,1 \;\; e^{j2\pi f_d T} \;\cdots\; e^{j2\pi f_d (N-1)T}\,\right]^T \\ &= Ae^{j\theta}\tilde{\boldsymbol{M}} \end{aligned} \tag{15.27}$$

where $\tilde{\boldsymbol{M}}$ is a vector representing the phase progression in the target signal due to the Doppler shift. Thus, to within a complex constant, $\tilde{\boldsymbol{M}}$ is a model of the expected signal structure for a target with a Doppler shift of f_d Hz. This vector is called a *steering vector* in Doppler. The total slow-time data $y[m]$ is $s[m]$ plus complex Gaussian noise $w[m]$:

$$y[m] = s[m] + w[m] \tag{15.28}$$

The SNR χ_1 of a single sample of $y[m]$ is A^2/σ_n^2, where σ_n^2 is the variance of the noise.

Again assuming the complex Gaussian noise case, the slow-time data vector $\boldsymbol{Y}$ is N independent samples of complex Gaussian noise under H_0. Their joint PDF is [2]

$$p_{\boldsymbol{Y}}(\boldsymbol{Y}|H_0) = \frac{1}{\pi^N \sigma_n^{2N}} \exp\left[-\frac{1}{\sigma_n^2}\boldsymbol{Y}^H\boldsymbol{Y}\right] \tag{15.29}$$

For the target-plus-noise case, the data are samples of complex Gaussian noise plus the target echo. Collecting the noise samples into a vector $\boldsymbol{W}$, the joint PDF of the data $\boldsymbol{Y} = \boldsymbol{S} + \boldsymbol{W}$ becomes

$$p_{\boldsymbol{Y}}(\boldsymbol{Y}|H_1,\theta) = \frac{1}{\pi^N \sigma_n^{2N}} \exp\left[-\frac{1}{\sigma_n^2}\left(\boldsymbol{Y} - Ae^{j\theta}\tilde{\boldsymbol{M}}\right)^H\left(\boldsymbol{Y} - Ae^{j\theta}\tilde{\boldsymbol{M}}\right)\right] \tag{15.30}$$

Expanding the exponent in (15.30) and defining the integrated signal energy $E = N \cdot A^2$ gives

$$\begin{aligned} p_{\boldsymbol{Y}}(\boldsymbol{Y}|H_1,\theta) &= \frac{1}{\pi^N \sigma_n^{2N}} \exp\left[-\frac{1}{\sigma_n^2}\left(\boldsymbol{Y}^H\boldsymbol{Y} - 2\mathrm{Re}\left\{Ae^{-j\theta}\tilde{\boldsymbol{M}}^H\boldsymbol{Y}\right\} + E\right)\right] \\ &= \frac{1}{\pi^N \sigma_n^{2N}} \exp\left[-\frac{1}{\sigma_n^2}\left(\boldsymbol{Y}^H\boldsymbol{Y} - 2A\left|\tilde{\boldsymbol{M}}^H\boldsymbol{Y}\right|\cos(\phi - \theta) + E\right)\right] \end{aligned} \tag{15.31}$$

where ϕ is the unknown, but fixed, phase of the inner product $\tilde{\boldsymbol{M}}^H\boldsymbol{Y}$ and the fact that $\tilde{\boldsymbol{M}}^H\tilde{\boldsymbol{M}} = N$ has been used.

It is important to note that the inner product $\tilde{\boldsymbol{M}}^H\boldsymbol{Y}$ represents *matched filtering* of the data samples $\boldsymbol{Y}$ with the target model represented by the steering vector $\tilde{\boldsymbol{M}}$. Writing this sum out explicitly and using equation (15.27) gives

$$\tilde{\boldsymbol{M}}^H\boldsymbol{Y} = \sum_{m=0}^{N-1} y[m]\,\tilde{\boldsymbol{M}}^*[m] = \sum_{m=0}^{N-1} y[m]\; e^{-j2\pi f_d mT} \tag{15.32}$$

Equation (15.32) is the discrete-time Fourier transform (DTFT) of the slow-time data $y[m]$. If the value of f_d assumed in the steering vector matches the actual value of the Doppler shift present in the data, then the operation $\tilde{\boldsymbol{M}}^H\boldsymbol{Y}$ implements coherent integration of the data. Specifically, if the data are of the form $y[m] = s[m] + w[m]$, where $s[m]$ is of the form given in (15.26) and $w[m]$ is complex Gaussian noise, the result of (15.32) becomes

$$\begin{aligned} \tilde{\boldsymbol{M}}^H\boldsymbol{Y} &= \sum_{m=0}^{N-1}\left(Ae^{j\theta}e^{+j2\pi f_d mT} + w[m]\right)\; e^{-j2\pi f_d mT} \\ &= NAe^{j\theta} + \sum_{m=0}^{N-1} w[m]\,e^{-j2\pi f_d mT} \\ &\equiv NAe^{j\theta} + w_N \end{aligned} \tag{15.33}$$

where w_N is a weighted sum of N complex Gaussian noise samples. The SNR, χ_N, of the matched filter output $\tilde{\boldsymbol{M}}^H\boldsymbol{Y}$ is increased by a factor of N relative to the single-sample case, to $NA^2/\sigma_n^2 = N\chi_1$. Thus, when the target component of the data can be modeled as having a known relative phase from one sample to the next, the LRT dictates coherent integration of that data!

Notice that $p_{\boldsymbol{Y}}(\boldsymbol{Y}|H_1, \theta)$ does indeed display an explicit dependence on θ. This dependence is removed by averaging over the PDF of the phase:

$$p_{\boldsymbol{Y}}(\boldsymbol{Y}|H_1) = \int p_y(\boldsymbol{Y}|H_1, \theta) p_\theta(\theta) d\theta. \tag{15.34}$$

Assuming a uniform random PDF for θ, defining $\theta' = \phi - \theta$, and applying (15.30) to (15.34) gives, after minor rearrangement,

$$p_{\boldsymbol{Y}}(\boldsymbol{Y}|H_1) = \frac{1}{\pi^N \sigma_n^{2N}} e^{-(\boldsymbol{Y}^H \boldsymbol{Y} + \boldsymbol{E})/\sigma_n^2} \frac{1}{2\pi} \int_0^{2\pi} \exp\left[\frac{2}{\sigma_n^2} |\tilde{\boldsymbol{M}}^H \boldsymbol{Y}| \cos\theta'\right] d\theta' \tag{15.35}$$

Equation (15.35) is a standard integral. Specifically, integral 9.6.16 in [10] is

$$\frac{1}{\pi} \int_0^{\pi} e^{\pm z \cos\theta} d\theta = I_0(z) \tag{15.36}$$

where $I_0(z)$ is the modified Bessel function of the first kind. Using this result and properties of the cosine function, equation (15.34) becomes

$$p_{\boldsymbol{Y}}(\boldsymbol{Y}|H_1) = \frac{1}{\pi^N \sigma_n^{2N}} e^{-(\boldsymbol{Y}^H \boldsymbol{Y} + \boldsymbol{E})/\sigma_n^2} I_0\left(\frac{2\left|\tilde{\boldsymbol{M}}^H \boldsymbol{Y}\right|}{\sigma_n^2}\right) \tag{15.37}$$

The log LRT now becomes

$$\ln \Lambda = \ln\left[I_0\left(\frac{2\left|\tilde{\boldsymbol{M}}^H \boldsymbol{Y}\right|}{\sigma_n^2}\right)\right] - \frac{E}{\sigma_n^2} \underset{H_0}{\overset{H_1}{\gtrless}} \ln T_\Lambda \tag{15.38}$$

or, equivalently,

$$\ln\left[I_0\left(\frac{2\left|\tilde{\boldsymbol{M}}^H \boldsymbol{Y}\right|}{\sigma_n^2}\right)\right] \underset{H_0}{\overset{H_1}{\gtrless}} \ln T_\Lambda + \frac{E}{\sigma_n^2} \equiv T' \tag{15.39}$$

Equation (15.39) defines the signal processing required for optimum detection in the presence of an unknown phase. It calls for taking the magnitude of the matched filter output $\tilde{\boldsymbol{M}}^H \boldsymbol{Y}$, passing it through the memoryless nonlinearity $\ln[I_0(\,)]$, and comparing the result with a threshold. This result is appealing in that the matched filter is still applied to utilize the *internal* phase structure of the known signal and get the maximum integration gain, but then a magnitude operation is applied because the absolute phase of the result can't be known. Again, the argument of the Bessel function is a signal-to-noise ratio.

As before, the same detection results can be obtained by simply comparing its argument $2\left|\tilde{\boldsymbol{M}}^H \boldsymbol{Y}\right| / \sigma_n^2$ with a modified threshold. Equation (15.39) then becomes simply

$$\left|\tilde{\boldsymbol{M}}^H \boldsymbol{Y}\right| \underset{H_0}{\overset{H_1}{\gtrless}} T \tag{15.40}$$

Figure 15-9 illustrates the optimal detector for the coherent detector with an unknown phase.

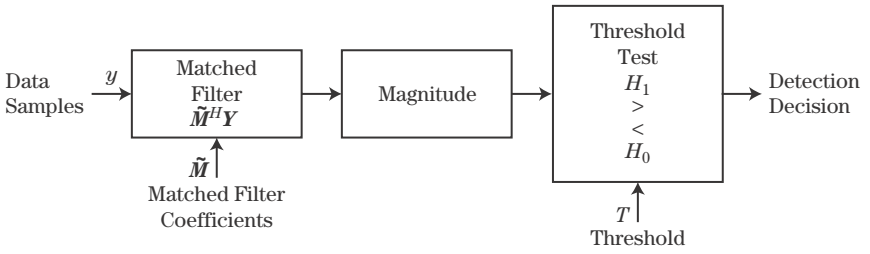

FIGURE 15-9 ■ Structure of optimal coherent detector.

Observe that equations (15.37) through (15.40) are essentially identical to equations (15.15) through (15.17) for the single-sample case but with $\left|\tilde{\boldsymbol{M}}^H\boldsymbol{Y}\right|$ substituted for $\tilde{m}|y|$ (and the scalar $\tilde{m}$ absorbed into the threshold in the single-sample case). This means that the performance of the optimal coherent detector will be the same as that of the optimal single-sample detector but with an SNR increased by the number of coherently integrated samples N. To confirm this, start by defining the detection statistic $z = |\tilde{\boldsymbol{M}}^H\boldsymbol{Y}|$. The detection test becomes simply $z \gtrless T$; thus the distribution of z under each of the two hypotheses is needed. As in the known phase case, under H_0 (target absent) $\tilde{\boldsymbol{M}}^H\boldsymbol{Y} \sim \mathrm{N}\left(0, E\sigma_n^2\right)$;[5] thus, the real and imaginary parts of $\tilde{\boldsymbol{M}}^H\boldsymbol{Y}$ are independent of one another and each is distributed as $\mathrm{N}\left(0, E\sigma_n^2/2\right)$. The detection statistic z is Rayleigh distributed:

$$p_z\left(z|H_0\right) = \begin{cases} \dfrac{2z}{E\sigma_n^2}\exp\left(-\dfrac{z^2}{E\sigma_n^2}\right), & z \geq 0 \\ 0, & z < 0 \end{cases} \tag{15.41}$$

The probability of false alarm is

$$P_{FA} = \int_T^{+\infty} p_z(z|H_0)dz = \exp\left(-\frac{T^2}{E\sigma_n^2}\right) \tag{15.42}$$

The threshold setting in terms of P_{FA} is

$$T = \sqrt{-E\sigma_n^2 \ln P_{FA}} \tag{15.43}$$

Now consider H_1, (i.e., target present). In this case $\tilde{\boldsymbol{M}}^H\boldsymbol{Y} \sim \mathrm{N}\left(E, E\sigma_n^2\right)$. Since E is real-valued, the real part $\tilde{\boldsymbol{M}}^H\boldsymbol{Y}$ is distributed as $\mathrm{N}\left(E, E\sigma_n^2/2\right)$ while the imaginary part is distributed as $\mathrm{N}\left(0, E\sigma_n^2/2\right)$. The PDF of z is

$$p_z\left(z|H_1\right) = \begin{cases} \dfrac{2z}{E\sigma_n^2}\exp\left[-\dfrac{1}{E\sigma_n^2}\left(z^2+E^2\right)\right] I_0\left(\dfrac{2z}{\sigma_n^2}\right), & z \geq 0 \\ 0, & z < 0 \end{cases} \tag{15.44}$$

[5]The notation $x \sim \mathrm{N}(\mu, \sigma^2)$ means that a random variable x is distributed normally (Gaussian) with mean μ and variance σ^2.

The probability of detection is obtained by integrating this Rician PDF from T to $+\infty$. The result can be expressed in terms of Marcum's Q function as

$$P_D = Q_M\left(\sqrt{\frac{2E}{\sigma_n^2}}\,,\ \sqrt{\frac{2T^2}{E\sigma_n^2}}\right) \tag{15.45}$$

Finally, noting that $E/\sigma_n^2 = NA^2/\sigma_n^2$ is the signal-to-noise ratio χ_N and expressing the threshold in terms of the false alarm probability using (15.20) gives

$$P_D = Q_M\left(\sqrt{2\chi_N}\,,\ \sqrt{-2\ln P_{FA}}\right) \tag{15.46}$$

Equation (15.46) is identical to equation (15.25), but with the single-sample SNR χ replaced by χ_N. Thus, as expected the performance is identical to that shown in Figure 15-7, provided the SNR is interpreted as the integrated SNR χ_N. This gives the important conclusion that single-sample detection performance results can be applied to the coherent integration case by simply using the coherently integrated SNR.

It is usually the case that the energy E in $\boldsymbol{S}$ or $\tilde{\boldsymbol{M}}$ and the noise power σ_n^2 are not known. Fortunately, equation (15.46) does not depend on them individually but only on their ratio χ_N so that it is possible to generate the ROC without this information. However, actually implementing the detector requires a specific value of the threshold T as given in equation (15.43), and this does require knowledge of both E and σ_n^2. One way to avoid this problem is to replace the matched filter coefficients $\tilde{\boldsymbol{M}}$ with a normalized coefficient vector $\hat{\boldsymbol{M}} = \tilde{\boldsymbol{M}}/E_{\tilde{\mathbf{m}}}$, where $E_{\tilde{\mathbf{m}}}$ is the energy in $\tilde{\boldsymbol{M}}$ (N in this example). This choice simply normalizes the gain of the matched filter to 1. The energy in this modified sequence $\hat{\boldsymbol{M}}$ is $\hat{E} = 1$, leading to a modified threshold

$$\hat{T} = \sqrt{-\sigma_n^2 \ln P_{FA}} \tag{15.47}$$

The reduced matched filter gain, along with the reduced threshold, results in no change to the ROC, so equation (15.46) remains valid. Setting of the threshold $\hat{T}$ still requires knowledge of the noise power, σ_n^2; removal of this restriction is the subject of Chapter 16.

15.5.5 Optimum Detector for a Nonfluctuating Target with Noncoherent Integration

Now consider detection based on noncoherent integration of N samples of a nonfluctuating target in white Gaussian noise. This is called the "Swerling 0," "Swerling 5," or "Marcum" case. Recall that "nonfluctuating" refers to the amplitude of the samples but does not imply that their phases have any known relationship. This model arises in several different types of radar detection problems. In the first, the N samples could be slow-time samples in a single CPI, as suggested by Figure 15-2d. Alternatively, they could be a single sample from each of N scans of a target region. The SNR of a single sample is denoted χ_1. In the second situation, some number of data samples are coherently integrated in each of N CPIs, and then the coherently integrated result from each of the CPIs are combined for detection without assuming any known phase relationship between the data from different CPIs. For example, pulse compression and Doppler DFTs could be applied to the data matrix for each CPI, and the N samples from a given range-Doppler cell could then be used to test for the presence of a target at that range and Doppler shift. This is the case

illustrated in Figure 15-2b. Another variation would be to coherently integrate in fast time only (pulse compression) and then to combine the results for a given range bin across slow time without assuming any particular slow-time phase relationship. This is the case illustrated for one of the two CPIs before threshold testing in Figure 15-2c. In the cases that include coherent integration, the SNR of the samples to be combined by noncoherent integration is $\chi_N = N\chi_1$.

Now consider detection based on the N available samples. The amplitude and absolute phase of the target component are unknown. Thus, an individual data sample y_n is again a complex constant $s = \tilde{m}\exp(j\theta)$ for some real amplitude $\tilde{m}$ and phase θ plus a white Gaussian noise sample of power $\sigma_n^2/2$ in each of the I and Q channels (total noise power σ_n^2). The PDFs of $z_n = |y_n|$ under H_0 (no target) and H_1 (target present) are again the Rayleigh and Rician densities of equations (15.19) and (15.22), respectively, with z replaced by z_n. For a vector $\boldsymbol{Z}$ of N such samples, the joint PDFs are, for each $z_n \geq 0$,

$$p_{\boldsymbol{Z}}(\boldsymbol{Z}|H_0) = \prod_{n=1}^{N} \frac{2z_n}{\sigma_n^2} \exp\left(-z_n^2/\sigma_n^2\right), \text{ and} \tag{15.48}$$

$$p_{\boldsymbol{Z}}(\boldsymbol{Z}|H_0) = \prod_{n=1}^{N} \frac{2z_n}{\sigma_n^2} \exp\left[-\left(z_n^2 + \tilde{m}^2\right)/\sigma_n^2\right] I_0\left(\frac{2\tilde{m}z_n}{\sigma_n^2}\right) \tag{15.49}$$

The LRT and log-LRT become

$$\begin{aligned}\Lambda &= \prod_{n=1}^{N} \exp\left(-\tilde{m}^2/\sigma_n^2\right) I_0\left(\frac{2\tilde{m}z_n}{\sigma_n^2}\right) \\ &= \exp\left(-\tilde{m}^2/\sigma_n^2\right) \prod_{n=1}^{N} I_0\left(\frac{2\tilde{m}z_n}{\sigma_n^2}\right) \underset{H_0}{\overset{H_1}{\gtrless}} T_\Lambda \end{aligned} \tag{15.50}$$

$$\ln\Lambda = -\frac{\tilde{m}^2}{\sigma_n^2} + \sum_{n=1}^{N} \ln\left[I_0\left(\frac{2\tilde{m}z_n}{\sigma_n^2}\right)\right] \underset{H_0}{\overset{H_1}{\gtrless}} \ln T_\Lambda \tag{15.51}$$

Incorporating the term involving the ratio of signal power and noise power on the left-hand side into the threshold gives

$$\sum_{n=1}^{N} \ln\left[I_0\left(\frac{2\tilde{m}z_n}{\sigma_n^2}\right)\right] \underset{H_0}{\overset{H_1}{\gtrless}} \ln(T_\Lambda) + \frac{\tilde{m}^2}{\sigma_n^2} \equiv T' \tag{15.52}$$

Equation (15.52) shows that, given N noncoherent samples of a nonfluctuating target in white noise, the optimal Neyman-Pearson detection test scales each sample by the quantity $2\tilde{m}/\sigma_n^2$, passes it through the monotonic nonlinearity $\ln[I_0(\cdot)]$, and then noncoherently integrates the processed samples and performs a threshold test. This result is very similar to the $N = 1$ case of equation (15.17). The integration is considered noncoherent because only the magnitude of the original data is being used; the phase information was discarded by the envelope detector.

There are three practical problems with this equation. First, as noted earlier, it is desirable to avoid computing the function $\ln[I_0(\cdot)]$ possibly millions of times per second. Second, both the target amplitude $\tilde{m}$ and the noise power σ_n^2 must be known to perform the required scaling. Third, performance analysis of the resulting detector would require

solving the difficult problem of finding the PDF of the sum of N samples of the transformed data $\ln\left[I_0\left(2\tilde{m}z_n/\sigma_n^2\right)\right]$, where z_n is the magnitude of a sample of either complex Gaussian noise, or complex Gaussian noise plus a constant target signal.

15.5.6 Linear and Square Law Detectors

It was noted in Section 15.5.3 that the $\ln[I_0(x)]$ function could be replaced by its argument x without altering the performance in the case of detection using a single sample ($N = 1$). When integrating $N > 1$ samples, a simpler detector characteristic is again desirable to simplify computation. While applying a monotonic increasing transformation to the right-hand side and to the entire summation on the left-hand side of (15.52) would not change the outcome of the comparison, this is not true in general if the transformation is applied instead to the individual $\ln[I_0(\cdot)]$ terms before the summation. However, it is possible to find a simpler alternate detector law by seeing what approximations can be made to the $\ln[I_0(\cdot)]$ function.

A standard series expansion for the Bessel function is $I_0(x) = 1 + x^2/4 + x^4/64 + \cdots$. Thus for small x, $I_0(x) \approx 1 + x^2/4$. Furthermore, one series expansion of the natural logarithm is $\ln(1+z) = z - z^2/2 + z^3/3 + \cdots$. Combining these gives

$$\ln[I_0(x)] \approx \frac{x^2}{4}, \quad x \ll 1 \tag{15.53}$$

Equation (15.53) shows that if x is small, the optimal detector is well approximated by a square law detector.

For large values of x, $I_0(x) \approx e^x \Big/ \sqrt{2\pi x}$, $x \gg 1$; then

$$\ln[I_0(x)] \approx x - \frac{1}{2}\ln(2\pi) - \frac{1}{2}\ln(x) \tag{15.54}$$

The constant term on the right of (15.54) can be incorporated into the threshold in equation (15.52), while the linear term in x quickly dominates the logarithmic term for $x \gg 1$. This leads to the linear detector approximation for large x:

$$\ln[I_0(x)] \approx x, \quad x \gg 1 \tag{15.55}$$

Figure 15-10 illustrates the fit between the square law and linear approximations and the exact $\ln[I_0(x)]$ function. The square law detector is an excellent fit for $10 \cdot \log_{10}(x) < 5$, while the linear detector fits the $\ln[I_0(x)]$ very well for $10 \cdot \log_{10}(x) > 10$.

Equations (15.53) and (15.55) show that, despite the summation, a linear or square law detector is still a close approximation to the optimal detection rule of equation (15.52). This is convenient since computation of these detectors is much simpler. Whether x is "big" or "small," and thus the choice of a linear or square law detector, depends not only on the actual signal strength but also on how that signal is digitized and numerically represented.

Finally, note that it is easy to compute the squared magnitude of a complex-valued test sample as simply the sum of the squares of the real and imaginary parts. The linear magnitude requires a square root and is less computationally convenient. A family of computationally simple approximations to the magnitude function is presented in [11].

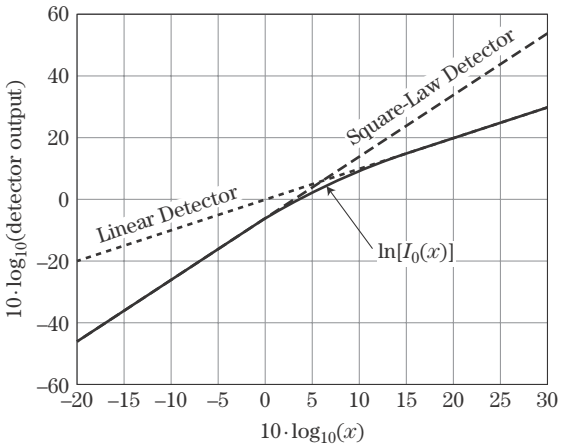

FIGURE 15-10 ■ Approximation of the $\ln[I_0(\cdot)]$ detector characteristic by the square law detector when its argument is small and the linear detector when its argument is large.

15.5.7 Square Law Detector Performance for a Nonfluctuating Target, $N > 1$

The test in equation (15.52) can now be simplified by applying the square law detector approximation of equation (15.53), giving the new test

$$\sum_{n=1}^{N} \frac{\tilde{m}^2 z_n^2}{\sigma_n^4} \underset{H_0}{\overset{H_1}{\gtrless}} T' \tag{15.56}$$

Combining the remaining constants into the threshold and defining the noncoherent sum z of the individual detected samples gives the final noncoherent integration detection rule:

$$z \equiv \sum_{n=1}^{N} z_n^2 \underset{H_0}{\overset{H_1}{\gtrless}} \frac{\sigma_n^4 T'}{\tilde{m}^2} \equiv T \tag{15.57}$$

Equation (15.57) states that the squared magnitudes of the data samples are simply integrated and the integrated sum compared with a threshold to decide whether a target is present.

The performance of the detector given in (15.57) must now be determined. It is convenient to scale the z_n, replacing them with the new variables $z_n' = z_n/\sigma_n$ and thus replacing z with $z' = \sum \left(z_n'\right)^2 = z/\sigma_n^2$; such a scaling does not change the performance but merely alters the threshold value that corresponds to a particular P_{FA}. The PDF of z_n' is still the Rayleigh voltage of equation (15.19) under H_0 or the Rician voltage of equation (15.22) under H_1, but now with unit noise variance. Since a square law detector is being used, the PDF of $y_n = \left(z_n'\right)^2$ is needed. This is exponential under H_0 and NCCS2 under H_1 (again with unit noise power) [2],

$$p_{y_n}(y_n|H_0) = \begin{cases} e^{-y_n}, & y_n \geq 0 \\ 0, & y_n < 0 \end{cases} \tag{15.58}$$

$$p_{y_n}(y_n|H_1) = \begin{cases} e^{-(y_n+\chi)} I_0\left(2\sqrt{\chi y_n}\right), & y_n \geq 0 \\ 0, & y_n < 0 \end{cases} \tag{15.59}$$

where $\chi = \tilde{m}^2/\sigma_n^2$ is the signal-to-noise ratio. Since z' is the sum of N scaled random variables $y_n = \left(z_n'\right)^2$, the PDF of z' is the N-fold convolution of the PDF given in equation (15.58) or (15.59).

In the H_0 case, the resulting PDF can be shown to be the Erlang density (a special case of the gamma density) [3]:

$$p_{z'}\left(z'|H_0\right) = \begin{cases} \dfrac{\left(z'\right)^{N-1}}{(N-1)!}e^{-z'}, & z' \geq 0 \\ 0, & z' < 0 \end{cases} \tag{15.60}$$

Note that this reduces to the exponential PDF when $N = 1$, as would be expected since in that case z' is the magnitude squared of a single sample of complex Gaussian noise. The probability of false alarm is obtained by integrating equation (15.60) from some threshold value to $+\infty$. The result is [1]

$$P_{FA} = \int_T^\infty \frac{(z')^{N-1}}{(N-1)!}e^{-z'}dz' = 1 - I\left(\frac{T}{\sqrt{N}}, N-1\right) \tag{15.61}$$

where

$$I(u, M) = \int_0^{u\sqrt{M+1}} \frac{e^{-\tau}\tau^M}{M!}d\tau \tag{15.62}$$

is Pearson's form of the incomplete gamma function. For a single sample ($N = 1$), equation (15.61) reduces to the especially simple result

$$P_{FA} = e^{-T} \tag{15.63}$$

so that $T = -\ln(P_{FA})$. Note that this value of threshold is the square of that found in equation (15.21) (with $\sigma_n = 1$), because this threshold is applied to the squared magnitude of the data samples whereas the earlier threshold was applied to just the linear magnitude of the data samples. Equation (15.63), which was also seen in Chapter 3, can be used to determine the probability of false alarm P_{FA} for a given threshold T or, more likely, to determine the required value of T for a desired P_{FA}.

Now the probability of detection, P_D, corresponding to the same threshold must be determined. Start by finding the PDF of the normalized, integrated, and square law detected samples under H_1. The result is [1,5]

$$p_{z'}\left(z'|H_1\right) = \left(\frac{z'}{N\chi}\right)^{(N-1)/2} e^{-z-N\chi} I_{N-1}\left(2\sqrt{N\chi z'}\right) \tag{15.64}$$

P_D is found by integrating equation (15.64). One version of the result, given in [12], is

$$\begin{aligned} P_D &= \int_T^\infty \left(\frac{z'}{N\chi}\right)^{(N-1)/2} e^{-z'-N\chi} I_{N-1}\left(2\sqrt{N\chi z'}\right) dz' \\ &= Q_M\left(\sqrt{2N\chi}, \sqrt{2T}\right) + e^{-(T+N\chi)} \sum_{r=2}^{N} \left(\frac{T}{N\chi}\right)^{(r-1)/2} I_{r-1}\left(2\sqrt{N\chi T}\right) \end{aligned} \tag{15.65}$$

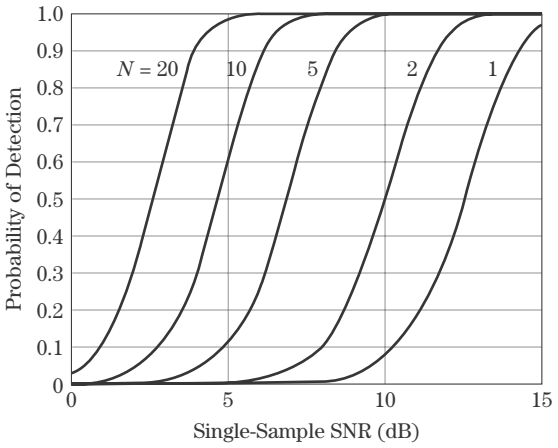

FIGURE 15-11 ■ Effect of noncoherent integration on detection performance for a nonfluctuating target in complex Gaussian noise.

The series term in this expression applies only when $N \geq 2$. Equations (15.61) and (15.65) define the performance achievable with noncoherent integration using a square law detector.

Figure 15-11 shows the effect of the number of samples noncoherently integrated, N, on the receiver operating characteristic. This figure shows that noncoherent integration reduces the single-sample SNR required to achieve a given P_D and P_{FA} but not by the factor N achieved with coherent integration. For example, consider the single-sample SNR required to achieve $P_D = 0.9$. For $N = 1$, this is 14.2 dB; for $N = 10$, it drops to 6.1 dB, a reduction of 8.1 dB, but less than the 10 dB that corresponds to the factor of 10 increase in the number of pulses integrated. In the next section a simple approximation for estimating this reduction in required single-sample SNR, called the *noncoherent integration gain*, will be developed.

It is important to realize that the noncoherent integration gain of 8.1 dB in the preceding example does not imply that the SNR of the square law detected and noncoherently integrated detection statistic z (or its linearly detected equivalent) is 8.1 dB higher than that of a single sample y. Because of the nonlinear magnitude-squared or magnitude operation, z cannot be expressed as the sum of separate noise and target contributions. Noncoherent integration gain represents the reduction in the SNR of the individual coherent data samples required to achieve certain values of P_D and P_{FA} when multiples samples are combined via noncoherent integration. Consequently, the noncoherent integration gain depends on the particular values of P_D and P_{FA} desired. It also depends on the SNR of the individual coherent samples.

15.5.8 Albersheim's Equation

The performance results for the case of N envelope-detected samples of a nonfluctuating target in complex Gaussian noise are given by equations (15.61) and (15.65). While relatively easy to implement in a modern software analysis system such as MATLAB, these equations do not lend themselves to hand calculation. Fortunately, there is a simple closed-form expression relating P_D, P_{FA}, and SNR that can be computed with simple scientific calculators. This expression is known as *Albersheim's equation* [13,14].

Albersheim's equation is an empirical approximation to the results in [5] for computing the single-sample SNR, χ_1, required to achieve a given P_D and P_{FA}. It applies under the

following conditions:

- Nonfluctuating target in Gaussian (IID in I and Q) noise.
- Linear (not square law) detector.
- Noncoherent integration of N samples.

The estimate is given by the series of calculations [13]

$$\begin{aligned} A &= \ln\left(\frac{0.62}{P_{FA}}\right) \\ B &= \ln\left(\frac{P_D}{1-P_D}\right) \\ \chi_{1_{\text{dB}}} &= -5\log_{10} N + \left(6.2 + \left(\frac{4.54}{\sqrt{N+0.44}}\right)\right) \cdot \log_{10}(A + 0.12AB + 1.7B) \ \text{dB} \end{aligned} \tag{15.66}$$

Note that $\chi_{1_{\text{dB}}}$ is in decibels, not linear power units. The error in the estimate of $\chi_{1_{\text{dB}}}$ is less than 0.2 dB for $10^{-7} \leq P_{FA} \leq 10^{-3}$, $0.1 \leq P_D \leq 0.9$, and $1 \leq N \leq 8096$ [13], a very useful range of parameters.

As a simple example of the use of Albersheim's equation, suppose $P_D = 0.9$ and $P_{FA} = 10^{-6}$ are required for a nonfluctuating target in a system using a linear detector. If detection is to be based on a single sample, what is the required SNR of that sample? Compute $A = \ln(0.62 \times 10^6) = 13.34$ and $B = \ln(0.9) = 2.197$. With $N = 1$, equation (15.66) then gives $\chi_{1_{\text{dB}}} = 13.14$ dB; on a linear scale, this is $\chi_1 = 20.59$.

If $N = 100$ samples are noncoherently integrated, it should be possible to obtain the same P_D and P_{FA} with a lower single-sample SNR. To confirm this, again apply Albersheim's equation but now with $N = 100$. The intermediate parameters A and B are unchanged. $\chi_{1_{\text{dB}}}$ is now reduced to -1.26 dB, a reduction of 14.4 dB. This noncoherent integration gain of 14.4 dB, a factor of 27.54 on a linear scale, is much better than the $\sqrt{N}$ rule of thumb sometimes given for noncoherent integration, which would give a gain factor of only 10 for $N = 100$ samples integrated. Rather, the gain is approximately $N^{0.7}$ in this example.

Albersheim's equation is useful because it requires no function more exotic than the natural logarithm and square root for its evaluation. It can thus be evaluated on virtually any scientific calculator. If a somewhat larger error can be tolerated, it can also be used for square law detector results for the nonfluctuating target, Gaussian noise case. Specifically, square law detector results are within 0.2 dB of linear detector results over a wide range of parameters [15,16]. Thus, the same equation can be used for calculations over the range of previously given parameters with errors not exceeding 0.4 dB.

Equation (15.66) provides for the calculation of χ_1 given P_D, P_{FA}, and N. It is possible, however, to solve (15.66) for either P_D or P_{FA} in terms of the other and χ_1 and N, extending further the usefulness of Albersheim's equation. For instance, the following calculations show how to estimate P_D given the other factors:

$$\begin{aligned} A &= \ln\left(\frac{0.62}{P_{FA}}\right), \quad Z = \frac{\chi_{1_{\text{dB}}} + 5\log_{10} N}{6.2 + \dfrac{4.54}{\sqrt{N+0.44}}}, \quad B = \frac{10^Z - A}{1.7 + 0.12A} \\ P_D &= \frac{1}{1+e^{-B}} \end{aligned} \tag{15.67}$$

In equation (15.67), A and B are the same values as in (15.66), though B cannot be computed in terms of P_D, since P_D is now the unknown. A result similar to (15.67) can be derived for computing P_{FA} in terms of P_D and $\chi_{1_{\text{dB}}}$.

Albersheim's equation can also be used to estimate the signal-to-noise ratio gain for noncoherent integration of N samples of a nonfluctuating target. The noncoherent integration gain is the reduction in single-sample SNR required to achieve a specified P_D and P_{FA} when N samples are combined. Coherent integration provides an integration gain of a factor of N, while noncoherent integration is less efficient, providing a gain of a factor of N^{α} for some $\alpha < 1$ (e.g., $\alpha \approx 0.7$ in the earlier example).

Figure 15-12a plots the value of α for the nonfluctuating, linear detector case, estimated using for Albersheim's equation with $P_D = 0.9$. The abscissa is the single-sample SNR, that is, the SNR before noncoherent integration. This figure shows that when the data are very noisy to begin with (single-sample SNR $\ll 0$ dB), the integration is inefficient, with α falling to about 0.55. (Note that $\alpha = 0.5$ would be a factor of $\sqrt{N}$.) If the data are very "clean" to begin with (single-sample SNR > 10 dB), α is in the neighborhood of 0.9. Since coherent integration corresponds to $\alpha = 1$, noncoherent integration is almost as efficient as coherent integration when the initial SNR is high. For lower values of P_D, the efficiency

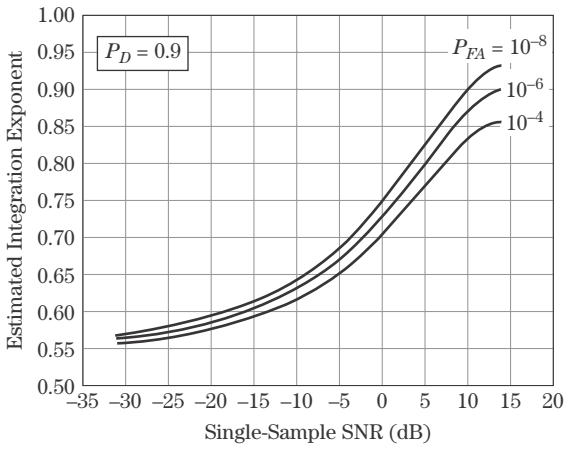

(a)

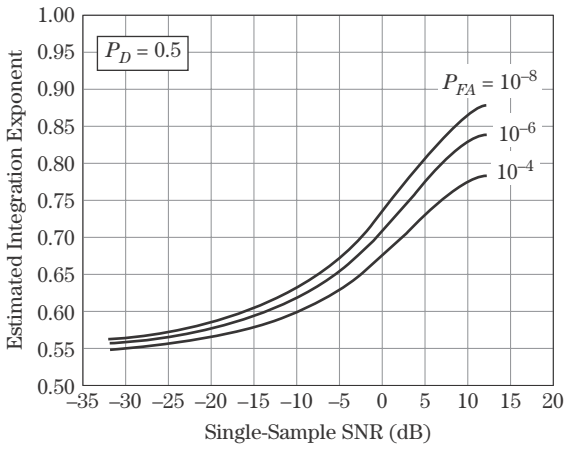

(b)

FIGURE 15-12 ■ Noncoherent integration gain exponent for a nonfluctuating target, estimated using Albersheim's equation.
(a) $P_D = 0.9$.
(b) $P_D = 0.5$.

falls somewhat for high-SNR data, as shown in Figure 15-12b, but never falls below $\sqrt{N}$ for low-SNR data.

15.5.9 Fluctuating Targets

The analysis in the preceding section considered only nonfluctuating targets, also called the "Swerling 0," "Swerling 5," or "Marcum" case. A more realistic model allows for target fluctuations, in which the target RCS is drawn from either the exponential or chi-square PDF, and the RCS of a group of N noncoherently integrated samples follows either the pulse-to-pulse or scan-to-scan decorrelation model, as described in Section 15.4.4. Note that representing the target by one of the Swerling models 1 through 4 has no effect on the probability of false alarm, since that is determined only by the PDF when no target is present; thus equation (15.61) still applies.

The strategy for determining probability of detection depends on the Swerling model used. Figure 15-13 illustrates the approach [5]. In all cases, the PDF of the magnitude of a single sample is still NCCS2, assuming a square law detector. However, the SNR χ is now a random variable because the target RCS is a random variable.

In the scan-to-scan decorrelation cases (Swerling models 1 and 3), the target RCS and thus SNR, while random, is the same value for all N pulses integrated to form z'. The PDF of a single sample is still given by equation (15.59). That result is then averaged over the SNR fluctuations to get an "average" PDF for the sum of N nonfluctuating target samples. For instance, in the Swerling 1 case, the PDF of the target RCS and therefore of the SNR is exponential:

$$p_\chi(\chi) = \frac{1}{\bar{\chi}} e^{-\chi/\bar{\chi}} \tag{15.68}$$

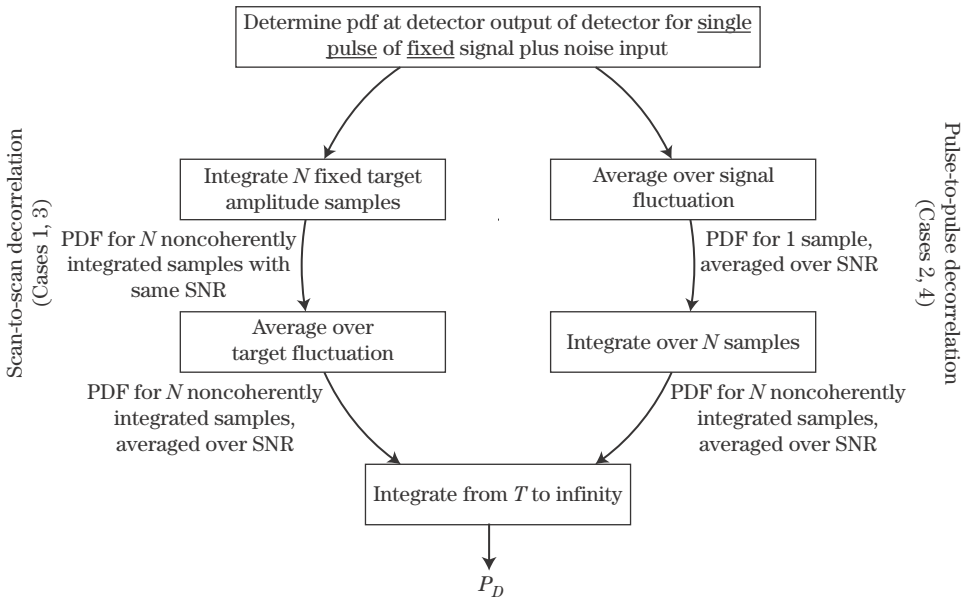

FIGURE 15-13 The strategy for computing P_D for fluctuating targets depends on the RCS fluctuation model.

where $\bar{\chi}$ is the average SNR over the N samples. The detailed calculations are beyond the scope of this chapter, but the resulting PDF of z' under H_1 is [1,12]

$$p_{z'}(z'|H_1) = \frac{1}{N\bar{\chi}}\left(1+\frac{1}{N\bar{\chi}}\right)^{N-2} I\left[\frac{z'}{(1+1/N\bar{\chi})\sqrt{N-1}}, N-2\right] e^{-z'/(1+N\bar{\chi})} \quad (15.69)$$

Integrating this PDF from the threshold T to $+\infty$ and assuming that $P_{FA} \ll 1$ and the integrated average SNR $N\bar{\chi} > 1$ (conditions that are almost always true in any scenario where target detection is likely to be successful) results in the following expression for the probability of detection in the Swerling 1 case [1,12]:

$$P_D \approx \left(1+\frac{1}{N\bar{\chi}}\right)^{N-1} e^{-T/(1+N\bar{\chi})}, \quad P_{FA} << 1, \quad N\bar{\chi} > 1 \quad (15.70)$$

Equation (15.70) is exact when $N = 1$; in this case it reduces to

$$P_D = \exp\left(-\frac{T}{1+\chi_1}\right), \quad N = 1 \quad (15.71)$$

(When there is only one pulse, the average SNR $\bar{\chi}$ is just the single-pulse SNR χ_1.) For the $N = 1$ case, equation (15.63) can then be used in (15.71) to write a direct relationship between P_D and P_{FA}:

$$P_D = (P_{FA})^{1/(1+\chi_1)} \quad (15.72)$$

This equation was seen also in Chapter 3.

In the Swerling 2 or 4 cases, the samples exhibit pulse-to-pulse decorrelation, meaning they are in fact uncorrelated with one another. In this case, each of the N samples integrated has a different value of SNR. The PDF of z' is therefore averaged over the SNR fluctuations first to get an "average" PDF for a single sample. The PDF of a detection statistic formed as the sum of N samples having that "average" PDF is then computed. The result is [1,12]

$$p_{z'}(z'|H_1) = \frac{z'^{N-1}\exp\left[z'/(1+\bar{\chi})\right]}{(1+\bar{\chi})^N (N-1)!}. \quad (15.73)$$

Integrating (15.73) gives the probability of detection, which can be shown to be [12]

$$P_D = 1 - I\left[\frac{T}{(1+\bar{\chi})\sqrt{N}}, N-1\right] \quad (15.74)$$

Results for Swerling 3 and 4 targets can be obtained by repeating the previously given analyses for the Swerling 1 and 2 cases, but with a chi-square instead of exponential density function for the SNR:

$$p_\chi(\chi) = \frac{4\chi}{\bar{\chi}^2} e^{-2\chi/\bar{\chi}} \quad (15.75)$$

Derivations of the resulting expressions for P_D can be found in [12,17] and many other radar detection texts. Table 15-2 summarizes one form of the resulting expressions.

Figure 15-14 compares the detection performance of the four Swerling model fluctuating targets and the nonfluctuating target for $N = 10$ samples as a function of the average single-sample SNR for a fixed $P_{FA} = 10^{-8}$. Assuming that the primary interest is in relatively high (> 0.5) values of P_D, the upper half of the figure is of greatest interest. In this case, the nonfluctuating target is the most favorable, in the sense that it achieves a given probability of detection at the lowest SNR. The worst case (highest required SNR

TABLE 15-2 ■ Probability of Detection for Swerling Model Fluctuating Targets with a Square Law Detector

Case	P_D	Comments
0 or 5	$Q_M(\sqrt{2N\bar{\chi}}, \sqrt{2T}) + e^{-(T+N\bar{\chi})} \sum_{r=2}^{N} \left(\frac{T}{N\bar{\chi}}\right)^{\frac{r-1}{2}} I_{r-1}(2\sqrt{NT\bar{\chi}})$	Second term applies only for $N \geq 2$
1	$\left(1 + \frac{1}{N\bar{\chi}}\right)^{N-1} e^{-T/(1+N\bar{\chi})}$	Approximate for $P_{FA} \ll 1$ and $N\bar{\chi} > 1$; exact for $N = 1$
2	$1 - I\left[\frac{T}{(1+\bar{\chi})\sqrt{N}}, N-1\right]$	
3	$\left(1 + \frac{2}{N\bar{\chi}}\right)^{N-2} \left[1 + \frac{T}{1+(N\bar{\chi}/2)} - \frac{2(N-2)}{N\bar{\chi}}\right] e^{-T/(1+(N\bar{\chi}/2))}$	Approximate for $P_{FA} \ll 1$ and $N\bar{\chi}/2 > 1$; exact for $N = 1$ or 2
4	$\left\{c^N \sum_{k=0}^{N} \frac{N!}{k!\,(N-k)!} \left(\frac{1-c}{c}\right)^{N-k}\right\} \left\{\sum_{l=0}^{2N-1-k} \frac{e^{-cT}\,(cT)^l}{l!}\right\}, \quad T > N(2-c)$ $1 - \left\{c^N \sum_{k=0}^{N} \frac{N!}{k!\,(N-k)!} \left(\frac{1-c}{c}\right)^{N-k}\right\} \left\{\sum_{l=2N-k}^{\infty} \frac{e^{-cT}\,(cT)^l}{l!}\right\}, \quad T < N(2-c)$	$c \equiv \frac{1}{1+(\bar{\chi}/2)}$
$P_{FA} = 1 - I\left(\frac{T}{\sqrt{N}}, N-1\right)$ in all cases		

$I(\cdot,\cdot)$ is Pearson's form of the incomplete Gamma function; $I_k(\cdot)$ is the modified Bessel function of the first kind and order k

Source: After Meyer and Mayer [12] (with permission).

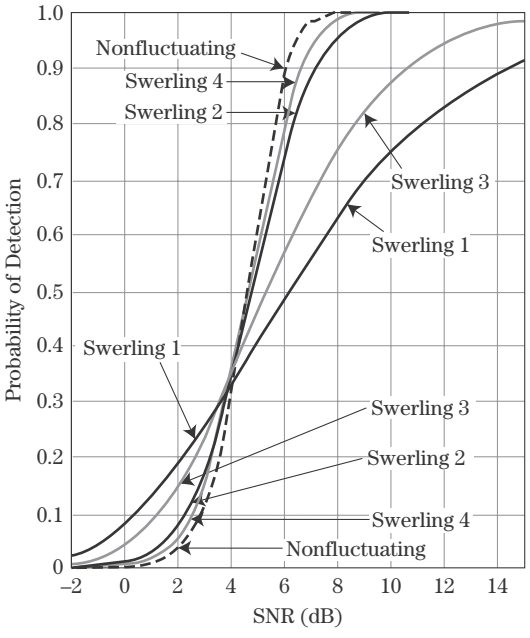

FIGURE 15-14 ■ Comparison of detection performance for fluctuating (Swerling) and nonfluctuating target models using noncoherent integration of $N = 10$ pulses and a fixed $P_{FA} = 10^{-8}$.

for a given P_D) is the Swerling case 1, which corresponds to scan-to-scan decorrelation and an exponential PDF for the target RCS. For instance, $P_D = 0.9$ requires $\bar{\chi} \approx 6$ dB for the nonfluctuating case, but $\bar{\chi} \approx 14.5$ dB for the Swerling 1 case, a difference of about 8.5 dB! This figure makes clear the fact that the assumed target model has a major impact on estimated detection performance.

At least two general conclusions can be drawn from this figure. First, for $P_D > 0.5$, nonfluctuating targets are easier to detect than any of the Swerling cases; target fluctuations make detection more difficult by requiring a higher SNR for a given P_D. Second, pulse-to-pulse fluctuations (Swerling 2 and 4) aid target detectability compared with scan-to-scan detectability. For instance, a Swerling 2 target is easier to detect than a Swerling 1 target that shares the same PDF for target fluctuations, and a Swerling 4 target is easier than a Swerling 3 target. Finally, note that the converse of these statements is true for detection probabilities less than about 0.35 in this case.

15.5.10 Frequency Agility

Figure 15-14 shows that, for reasonably high signal-to-noise ratios, the probability of detection is higher for Swerling 2 or 4 targets than it is for Swerling 1 or 3 targets. This suggests that if the target RCS is going to fluctuate, it is preferable to have pulse-to-pulse fluctuations. If the radar-to-target aspect angle does not change enough during the CPI to decorrelate the target echoes, the radar can take advantage of the fact that changing the radar frequency will decorrelate the measurements. As was discussed in Section 15.4.3, the technique of changing the radar frequency pulse-to-pulse to improve detection performance is called *frequency agility*.[6] The frequency step required to decorrelate a complex target was given in equation (15.13) as approximately $\Delta f = c/2L_d$, where L_d is the depth of the target projected along the radar boresight. The required frequency step size is typically a few tens of megahertz.

15.5.11 Shnidman's Equation

Albersheim's equation provided a simple way to compute the single-sample SNR required to achieve a specified P_D and P_{FA} for a nonfluctuating target and a linear detector or, with slightly greater error, a square law detector, over a useful range of parameters. Furthermore, it can be rearranged to solve for P_D (or P_{FA}) in terms of N, SNR_1, and P_{FA} (or P_D). While an extremely useful tool, Albersheim's equation has the serious limitation that it does not treat the case of fluctuating targets. As was seen in Figure 15-14, the nonfluctuating case is optimistic, especially compared with cases characterized by scan-to-scan decorrelation behavior.

Recently, a new empirical approximation has been developed that addresses this limitation. *Shnidman's equation*, like Albersheim's, is an analytically based but ultimately empirical approximation to compute the required single-sample SNR to achieve a specified P_D and P_{FA} when N pulses are noncoherently integrated [18]. However, it applies to all four Swerling models.

Though somewhat lengthier to express than Albersheim's equation, the actual calculation are equally simple. It begins by selecting values for the parameters K and α; the

[6]The term *frequency agility* generally implies changing the radar frequency for the purpose of improving detection. When this is done for electronic counter-countermeasure (antijamming) purposes, it is generally called *frequency diversity*.

choice of K determines the Swerling model to be represented. Two derived parameters η and X_∞ are then computed:[7]

$$K = \begin{cases} \infty, & \text{nonfluctuating target (“Swerling 0/5”)} \\ 1, & \text{Swerling 1} \\ N, & \text{Swerling 2} \\ 2, & \text{Swerling 3} \\ 2N, & \text{Swerling 4} \end{cases}$$

$$\alpha = \begin{cases} 0, & N < 40 \\ \dfrac{1}{4}, & N \geq 40 \end{cases} \tag{15.76}$$

$$\eta = \sqrt{-0.8 \ln\left(4P_{FA}\left(1 - P_{FA}\right)\right)} + \text{sign}\left(P_D - 0.5\right)\sqrt{-0.8 \ln\left(4P_D\left(1 - P_D\right)\right)}$$

$$X_\infty = \eta\left[\eta + 2\sqrt{\frac{N}{2} + \left(\alpha - \frac{1}{4}\right)}\right]$$

Next, the series of constants C_1, C_2, C_{dB}, and C are computed:

$$C_1 = \left\{\left[\left(17.7006P_D - 18.4496\right)P_D + 14.5339\right]P_D - 3.525\right\} \Big/ K$$

$$C_2 = \frac{1}{K}\left\{\exp\left(27.31P_D - 25.14\right) + \left(P_D - 0.8\right)\left[0.7 \ln\left(\frac{10^{-5}}{P_{FA}}\right) + \frac{(2N - 20)}{80}\right]\right\}$$

$$C_{dB} = \begin{cases} C_1, & 0.1 \leq P_D \leq 0.872 \\ C_1 + C_2, & 0.872 < P_D \leq 0.99 \end{cases}$$

$$C = 10^{C_{dB}/10} \tag{15.77}$$

Notice that C_1 and C_2 will equal 0, and therefore C equals 1, for the nonfluctuating case. Finally,

$$\chi_1 = \frac{C \cdot X_\infty}{N}$$

$$\chi_{1_{dB}} = 10 \log_{10}(SNR_1) \tag{15.78}$$

Equations (15.76) through (15.78) constitute Shnidman’s equation.

The accuracy of these equations is better than 1 dB for the parameter range $0.1 \leq P_D \leq 0.99$, $10^{-9} \leq P_{FA} \leq 10^{-3}$, and $1 \leq N \leq 100$, with the error being less than 0.5 dB over nearly all of this parameter range. (A variant is given in [18] that maintains the same accuracy for values of P_D up to 0.9992 if N is restricted to 20 or less.) The greatest errors occur for the Swerling 1 case near the two extremes of P_D. Compared to Albersheim’s equation, this is a more restricted but still very useful range of N, but a significantly better

[7]The function sign(x) equals 1 if the argument $x \geq 0$ and -1 if $x < 0$.

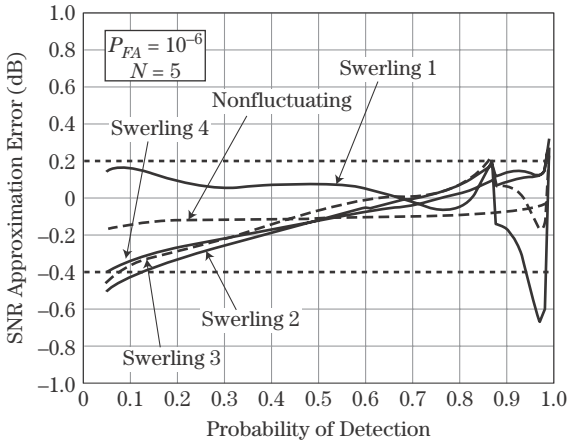

FIGURE 15-15 ■ Example of error in Shnidman's approximation.

upper limit on P_D (0.99 instead of 0.9), at the expense of a looser error bound (0.5 to 1 dB instead of 0.2 dB). Figure 15-15 plots a representative set of approximation error curves for the various Swerling cases for the particular case of $N = 5$ and $P_{FA} = 10^{-6}$. While Shnidman's equation applies directly only to a square law detector, the same argument used to extend Albersheim's equation to both detector types, at the cost of an increase in error of about 0.2 dB, can be applied to extend Shnidman's equation to linear detectors with a similar error increase.

15.5.12 Detection in Clutter

The specific results derived in the previous sections, for both nonfluctuating and fluctuating targets, all assumed that the interference was complex, white Gaussian noise. While appropriate for many radar systems and also for cases where noise jammers are the dominant interference, in many other systems the dominant interference is clutter, not noise. The probability density function of a single sample of envelope-detected clutter, discussed in Chapter 5, is often not well modeled by the Rayleigh voltage/exponential power function that describes noise. A very wide variety of models are described in the literature; see the book by Long [19] for an excellent introduction.

In addition to changes in the single-sample PDFs, the decorrelation models used to describe clutter are often complex, primarily because they are functions not only of radar-clutter geometry but, in many cases, of such factors as weather and the seasons. For example, tree clutter decorrelates faster when the wind speed increases due to increased movement of the branches and leaves. Furthermore, deciduous tree clutter statistics vary drastically between summer, when the branches are fully leafed out, and winter when they are bare. These changes affect the clutter reflectivity and PDFs as well as the decorrelation behavior.

Despite these difficulties, the basic procedure for determining detection performance in clutter is the same as described here; the difference is that the PDFs $p_y(y|H_0)$ and $p_y(y|H_1)$ will change, leading to new likelihood ratios and detection statistics, and new ROC equations. In practice, non-Gaussian PDFs usually lead to more difficult calculations, though results are available for many specific models in the literature. Good examples of studies of coherent detection in non-Gaussian clutter are available in [20–22].

15.5.13 Binary Integration

If the entire threshold detection process is repeated n times, n binary decisions will be available. Binary integration was discussed in some detail in Chapter 3. The detection probability of a properly implemented binary integration detector is higher than the P_D obtained on a single detection test. Conversely, the P_{FA} is lower than the single-test P_{FA}. Thus, the binary integration technique can improve both detection and false alarm performance. Alternatively, the single-dwell P_D and P_{FA} requirements can be relaxed while still meeting the overall performance specification. Examples are given in Chapter 3.

The analysis in Chapter 3 implicitly assumes a nonfluctuating target, since the single-trial P_D was assumed to be the same on each trial. The results can be extended to fluctuating targets [23,24]; these studies also indicate optimum choices for m as a function of the target model and n. Finally, other binary integration strategies exist with somewhat different properties; for instance, the decision logic can require that the m hits be contiguous rather than just any m hits out of n. See [25] for references to the literature for these and other variations on binary integration.

15.6 FURTHER READING

An excellent concise reference for modern detection theory is Chapter 5 of the text by Johnson and Dudgeon [26]. When greater depth is needed, another excellent modern reference with a digital signal processing point of view is volume II of Kay's text [2]. An important classical textbook in detection theory is Part I of Van Trees's series [27], while Meyer and Mayer [12] and DiFranco and Rubin [17] provide classical in-depth analyses and many detection curves specifically for radar applications. A good recent source on basic radar detection models and calculations is the series of papers by Shnidman [6,8,16,23].

15.7 REFERENCES

[1] Richards, M.A., *Fundamentals of Radar Signal Processing*, McGraw-Hill, New York, 2005.

[2] Kay, S.M., *Fundamentals of Statistical Signal Processing, Vol. II: Detection Theory,* Prentice-Hall, Upper Saddle River, NJ, 1998.

[3] Papoulis, A., and Pillai, S.U., *Probability, Random Variables, and Stochastic Processes*, 4th ed., McGraw-Hill, New York, 2002.

[4] Ray, H., "Improving Radar Range and Angle Detection with Frequency Agility," *Microwave Journal,* pp. 64ff, May 1966.

[5] Swerling, P., "Probability of Detection for Fluctuating Targets," *IRE Trans. Information Theory*, vol. IT-6, pp. 269–308, April 1960.

[6] Shnidman, D.A., "Calculation of Probability of Detection for Log-Normal Target Fluctuations," *IEEE Trans. Aerospace and Electronic Systems*, vol. AES-27, no. 1, pp. 172–174, January 1991.

[7] Swerling, P., "Radar Probability of Detection for Some Additional Fluctuating Target Cases," *IEEE Trans. Aerospace and Electronic Systems*, vol. AES-33, no. 2, pp. 698–708, April 1997.

[8] Shnidman, D.A., "Expanded Swerling Target Models," *IEEE Transactions on Aerospace and Electronic Systems*, vol. AES-39, no. 3, pp. 1059–1068, July 2003.

[9] Cantrell, P.E., and Ojha, A.K., "Comparison of Generalized *Q*-Function Algorithms," *IEEE Trans. Information Theory*, vol. IT-33, no. 4, pp. 591–596, July 1987.

[10] Abramowitz, M., and Stegun, I.A., *Handbook of Mathematical Functions: with Formulas, Graphs, and Mathematical Tables*, U.S. National Bureau of Standards, Applied Mathematics Series – 55, Washington, DC, 1964.

[11] Filip, A.E., "A Baker's Dozen Magnitude Approximations and Their Detection Statistics," *IEEE Trans. Aerospace & Electronic Systems*, pp. 86–89, January 1976.

[12] Meyer, D.P., and Mayer, H.A., *Radar Target Detection*, Academic Press, New York, 1973.

[13] Albersheim, W.J., "Closed-Form Approximation to Robertson's Detection Characteristics," *Proceedings IEEE*, vol. 69, no. 7, p. 839, July 1981.

[14] Tufts, D.W., and Cann, A.J., "On Albersheim's Detection Equation," *IEEE Trans. Aerospace and Electronic Systems*, vol. AES-19, no. 4, pp. 643–646, July 1983.

[15] Robertson, G.H., "Operating Characteristic for a Linear Detector of CW Signals in Narrow Band Gaussian Noise," *Bell System Technical Journal*, vol. 46, no. 4, pp. 755–774, April 1967.

[16] Shnidman, D.A., "Radar Detection Probabilities and Their Calculation," *IEEE Transactions on Aerospace and Electronic Systems*, vol. AES-31, no. 3, pp. 928–950, July 1995.

[17] DiFranco, J.V., and Rubin, W.L., *Radar Detection,* Artech House, Dedham, MA, 1980.

[18] Shnidman, D.A., "Determination of Required SNR Values," *IEEE Trans. Aerospace & Electronic Systems*, vol. AES-38, no. 3, pp. 1059–1064, July 2002.

[19] Long, M.W., *Radar Reflectivity of Land and Sea*, Artech House, Dedham, MA, 2001.

[20] Gini, F., "Sub-optimum Coherent Radar Detection in a Mixture of K-distributed and Gaussian Clutter," *Proc. IEE Radar, Sonar and Navigation,* vol. 144, no. 1, pp. 39–48, February 1997.

[21] Sangston, K.J., and Gerlach, K.R., "Coherent Detection of Radar Targets in a Non-Gaussian Background," *IEEE Trans. Aerospace & Electronic Systems*, vol. AES30, no. 2, pp. 330–340, April 1994.

[22] Sangston, K.J., Gini, F., Greco, M.V., and Farina, A., "Structures for Radar Detection in Compound Gaussian Clutter," *IEEE Trans. Aerospace & Electronic Systems*, vol. AES35, no. 2, pp. 445–458, April 1999.

[23] Shnidman, D.A., "Binary Integration for Swerling Target Fluctuations," *IEEE Trans. Aerospace & Electronic Systems*, vol. AES-34, no. 3, pp. 1043–1053, July 1998.

[24] Weiner, M.A., "Binary Integration of Fluctuating Targets," *IEEE Trans. Aerospace & Electronic Systems*, vol. AES-27, no. 1, pp. 11–17, July 1991.

[25] Skolnik, M.I., *Introduction to Radar Systems*, 3d ed., McGraw-Hill, New York, 2001.

[26] Johnson, D.H., and Dudgeon, D.E., *Array Signal Processing*, Prentice-Hall, Englewood Cliffs, NJ, 1993.

[27] Van Trees, H.L., *Detection, Estimation, and Modulation Theory, Part I: Detection, Estimation, and Linear Modulation Theory,* Wiley, New York, 1968.

15.8 PROBLEMS

1. Consider detection of a real-valued constant in zero-mean real-valued Gaussian noise. Let the noise variance $\sigma_n^2 = 2$, the number of samples $N = 1$, and the constant $m = 4$. What is the SNR for this case? Sketch approximately the distributions $p(y|H_0)$ and $p(y|H_1)$; be sure to label appropriate numerical values on the axes.

2. Write the likelihood ratio and log-likelihood ratio that applies to problem 1. Simplify the resulting expressions.

3. Continuing with the same parameters given in problem 1, what is the required value of the threshold T to achieve $P_{FA} = 0.01$ (1%)? Look-up tables or MATLAB can be used to calculate the values of functions such as erf(·), erfc(·), $\text{erf}^{-1}(\cdot)$, or $\text{erfc}^{-1}(\cdot)$ that may be needed.

4. With the threshold selected in problem 3, what is the resulting value of P_D? Look-up tables or MATLAB can be used to calculate the values of functions such as erf(·), erfc(·), $\text{erf}^{-1}(\cdot)$, or $\text{erfc}^{-1}(\cdot)$ that may be needed.

5. Suppose m from problem 1 is increased to double the SNR on a linear (not dB) scale; $\sigma_n^2 = 2$ and $N = 1$ still. What is the new value of m? Sketch approximately the distributions $p(y|H_0)$ and $p(y|H_1)$ with this new value of m; be sure to label appropriate numerical values on your axes.

6. If the same value of the threshold T found in problem 3 is retained when m is increased to the value in problem 5, does the P_{FA} change, and, if so, what is the new value?

7. If the same value of the threshold T found in found in problem 3 is retained when m is increased to the value in problem 5, does the P_D change, and, if so, what is the new value?

8. Go back to the case of $m = 4$, but now reduce the noise variance to $\sigma_n^2 = 1$. $N = 1$ still. What is the SNR now? Again, sketch approximately the distributions $p(y|H_0)$ and $p(y|H_1)$ with this value of m and σ_n^2; be sure to label appropriate numerical values on the axes.

9. Assuming the same threshold T from problem 3 is maintained with the values of m and σ_n^2 from problem 8, does the P_{FA} change from the value in problem 3, and, if so, what is the new value?

10. If the same value of the threshold T is retained with the values of m and σ_n^2 from problem 8, does the P_D change from the value in problem 4, and, if so, what is the new value?

11. Compute the threshold T and probability of detection P_D for the case of a constant in zero-mean complex Gaussian noise, but now with *unknown phase*. Use $\tilde{m} = 4$, $\sigma_n^2 = 2$, $N = 1$, and $P_{FA} = 0.01$ again. It will be necessary to evaluate the Marcum Q function Q_M. The website for this book includes a MATLAB routine marcum that can be used for the numerical evaluation.

12. Use Albersheim's equation to estimate the single-sample SNR χ_1 required to achieve $P_{FA} = 0.01$ and P_D equal to the same value obtained in problem 11. How does the result compare with the actual SNR in problem 1?

13. Repeat problem 12 using Shnidman's equation in place of Albersheim's equation.

14. Using the PDFs for the case of a nonfluctuating target in complex Gaussian noise given by equations (15.14) and (15.15), derive the LRT of equation (15.17).

15. Coherently integrating N samples of signal-plus-noise produces an integration gain of N on a linear (not dB) scale; that is, if the SNR of a single sample y_i is χ, the SNR of $z = \sum_{i=1}^{N} y_i$ is $N\chi$. It is also often said that *non*coherent integration produces an integration gain of about $\sqrt{N}$. In problems 15 through 18, Albersheim's equation will be used to see if this is accurate for one example case. Throughout these problems, assume $P_D = 0.9$ and $P_{FA} = 10^{-6}$ is required and that a linear (not square law) detector is used. Start by considering detection based on a single sample, $N = 1$. Use Albersheim's equation to estimate the signal-to-noise ratio, χ_1, needed for this single sample to meet the previously given specifications. Give the answer in dB. Be careful about comparing or combining things on the same (linear or dB) scales throughout these four related problems.

16. Continuing, suppose the system now noncoherently integrates 100 samples to achieve the same P_D and P_{FA}. Each individual sample can then have a lower SNR. Use Albersheim's equation

again to estimate the signal-to-noise ratio χ_{nc} in dB of each sample needed to achieve the required detection performance.

17. Continuing, now consider *coherent* integration of 100 pulses. What is the signal-to-noise ratio χ_c required, in dB, for each sample such that the coherently integrated SNR will be equal to the value χ_1 found in problem 8?

18. Finally, the noncoherent integration gain is the ratio χ_1/χ_{nc}, where χ_1 and χ_{nc} are on a linear (not dB) scale. To compare it with the $\sqrt{N}$ estimate, find α such that $\chi_1/\chi_{nc} = N^{\alpha}$. Is the noncoherent integration gain better or worse than $\sqrt{N}$ in this case? Is it better or worse than coherent integration?

19. Rearrange Albersheim's equation to derive a set of equations for P_{FA} in terms of P_D, N, and single-pulse SNR in dB, χ_1.

20. Use Shnidman's equation to estimate the single-pulse SNR χ_1 in dB required to achieve $P_{FA} = 10^{-8}$ and $P_D = 0.9$ when noncoherently integrating $N = 10$ samples. Do this for all four Swerling cases and for the nonfluctuating case. (*Hint*: The answers should match the data in Figure 15-14.)